AGU PUBLICATIONS

Geochemistry, Geophysics, Geosystems

RESEARCH ARTICLE
10.1002/2013GC004993

Special Section:
Oceanic detachment faults

Magnetic properties of variably serpentinized peridotites and their implication for the evolution of oceanic core complexes

Marco Maffione[1], Antony Morris[2], Oliver Plümper[1], and Douwe J. J. van Hinsbergen[1]

[1]Department of Earth Sciences, Utrecht University, Utrecht, Netherlands, [2]School of Geography, Earth and Environmental Sciences, Plymouth University, Plymouth, UK

Key Points:
- Magnetic properties of variably serpentinized peridotite are investigated
- Abyssal peridotites are unlikely to contribute to marine magnetic anomalies
- A new conceptual model for serpentinization at OCCs is proposed

Supporting Information:
- Read me
- Tables S1 and S2

Correspondence to:
M. Maffione,
m.maffione@uu.nl

Citation:
Maffione, M., A. Morris, O. Plümper, and D. J. J. van Hinsbergen (2014), Magnetic properties of variably serpentinized peridotites and their implication for the evolution of oceanic core complexes, *Geochem. Geophys. Geosyst.*, *15*, 923–944, doi: 10.1002/2013GC004993.

Received 9 AUG 2013
Accepted 3 FEB 2014
Accepted article online 8 FEB 2014
Published online 2 APR 2014

Abstract Serpentinization of ultramafic rocks during hydrothermal alteration at mid-ocean ridges profoundly changes the physical, chemical, rheological, and magnetic properties of the oceanic lithosphere. There is renewed interest in this process following the discovery of widespread exposures of serpentinized mantle on the seafloor in slow spreading oceans. Unroofing of mantle rocks in these settings is achieved by displacement along oceanic detachment faults, which eventually results in structures known as oceanic core complexes (OCCs). However, we have limited understanding of the mechanisms of serpentinization at the seafloor and in particular their relationship with the evolution of OCCs. Since magnetite is a direct product of serpentinization, the magnetic properties of variably serpentinized peridotites can provide unique insights into these mechanisms and their evolution in the oceanic lithosphere. Here we present new results from an integrated, rock magnetic, paleomagnetic, and petrological study of variably serpentinized peridotites from the first fossil OCC recognized in an ophiolite. Integration with existing data from mid-ocean ridge-related abyssal peridotites recovered from several scientific ocean drilling sites yields the first magnetic database from peridotites extending across the complete range (0–100%) of degrees of serpentinization. Variations in a range of magnetic parameters with serpentinization, and associated paleomagnetic data, provide: (i) key constraints on the mechanism(s) of serpentinization at mid-ocean ridges; (ii) insights on the potential for serpentinized peridotites to contribute to marine magnetic anomalies; and (iii) evidence that leads to a new conceptual model for the evolution of serpentinization and related remanence acquisition at OCCs.

1. Introduction

At slow and ultraslow spreading ridges (<4 cm/yr) like the Mid-Atlantic Ridge (MAR), up to 80% of plate divergence may be accommodated by low-angle, large-offset extensional (detachment) faults [*Escartín et al*., 2008; *Smith et al*., 2008; *Grimes et al*., 2008; *Baines et al*., 2008]. This tectonic style has recently been recognized as an alternative "detachment-mode" of seafloor spreading [e.g., *Escartín and Canales*, 2011], representing one of the major advances in understanding plate tectonics in the last three decades. Detachment faults are responsible for the exhumation of upper mantle and lower oceanic crust to the ocean floor, and may lead to the formation of uplifted, domal structures known as oceanic core complexes (OCCs) [*Cannat et al*., 1995; *Cann et al*., 1997; *Tucholke et al*., 1998; *Blackman et al*., 2006; *MacLeod et al*., 2002, 2009; *Ildefonse et al*., 2007]. In addition to unroofing of upper mantle rocks by displacement on oceanic detachment faults, in ultraslow, melt-poor settings (e.g., along the Southwest Indian Ridge) serpentinized mantle peridotites are exposed over large expanses of seafloor, with no evidence for a volcanic upper crustal layer (generating so-called "smooth seafloor") [*Cannat et al*., 2006, 2008; *Sauter et al*., 2013]. Exposure of mantle rocks on the seafloor has also been documented in hyper-extended, magma-poor rifted margins (e.g., associated with the opening of the Piemonte-Ligurian ocean) [*Beltrando et al*., 2012; *Mohn et al*., 2012; *Vissers et al*., 2013].

A key process within these various systems, having fundamental repercussions for the structure and mechanics of the oceanic lithosphere and thereby its response to geodynamic processes, is seawater-induced alteration of mafic and ultramafic rocks triggering a sequence of metamorphic hydration reactions known as serpentinization [e.g., *Moody*, 1976; *O'Hanley*, 1996]. This alteration process has a profound impact on magnetic properties [*Toft et al*., 1990; *Bina and Henry*, 1990; *Dyment et al*., 1997; *Oufi et al*., 2002], rheology [*Escartín et al*., 1997, 2001], gravity and seismic structure [*Christensen*, 1978], and the geochemical budget [*Thompson and Melson*, 1970; *Snow and Dick*, 1995] of the oceanic lithosphere, but also aids

microbial processes at deep-sea hydrothermal vents [*Alt and Shanks*, 1998; *Kelley et al*., 2001; *Ménez et al*., 2012]. Serpentinization-induced production of ferromagnetic minerals (i.e., magnetite), and the subsequent acquisition of a magnetic remanence by the altered ultramafic and mafic rocks, may have direct implications for the origin of oceanic magnetic anomalies [*Dyment et al*., 1997; *Nazarova*, 1994; *Allerton and Tivey*, 2001; *Gee and Kent*, 2007]. Considering the widespread occurrence of peridotites at the seafloor, a detailed description of the magnetic properties of such lithologies is essential to correctly interpret the different sources of magnetic anomalies within the oceanic lithosphere. Moreover, the variation of magnetic parameters with serpentinization provides a unique proxy to investigate this key, but poorly understood, alteration process.

Here we explore the changes of paleomagnetic, rock magnetic, and petrological properties within variably serpentinized peridotites from a fossil OCC identified recently in the Jurassic Mirdita ophiolite of Albania [*Nicolas et al*., 1999; *Tremblay et al*., 2009; *Maffione et al*., 2013]. Our results, combined with a compilation of 239 modern, mid-ocean ridge-related abyssal peridotite samples (hereinafter called "MAP"; supporting information text S1) from DSDP sites 395, 558, 560, and ODP sites 670, 895B/C/D/E, 920B/D, 1268A, 1270A/C/D, 1271A/B, 1272A, and 1274A [*Oufi et al*., 2002; *Kelemen et al*., 2004; *Klein et al*., 2014], provide the most complete database of magnetic properties of variably serpentinized peridotites (0–100% serpentinization). The analysis of this combined database provides insights into: (i) the main features and products of serpentinization; (ii) the role of serpentinization in the development of marine magnetic anomalies; and (iii) the evolution of serpentinization and its effects on magnetic remanences during detachment-mode seafloor spreading.

2. Serpentinization of Ultramafic Rocks

Serpentinization of ultramafic rocks is a low-temperature, fluid-mediated hydration process (200–400°C) that commonly evolves under static and highly reducing conditions [*Moody*, 1976; *O'Hanley*, 1996; *Mével*, 2003; *Evans*, 2004; *Bach et al*., 2004, 2006; *Frost and Beard*, 2007; *Beard et al*., 2009; *Frost et al*., 2013]. In a simple (nonbalanced) form the serpentinization reaction can be described as:

$$\text{Olivine} \pm \text{Pyroxene} + \text{Water} = \text{Serpentine} + \text{Brucite} \pm \text{Magnetite} \pm \text{Talc} \pm \text{Tremolite} + \text{Hydrogen} \quad (1)$$

The entire serpentinization process develops through multiple reactions depending on the fluid-rock alteration environment. In a rock-dominated system, where water influx is limited and the activity of iron, magnesium and silica is controlled by the original rock composition, thin (50–100 μm) "Type 1" veins of iron-rich serpentine (lizardite) and brucite form [*Frost and Beard*, 2007; *Beard et al*., 2009; *Frost et al*., 2013]. Whether significant amounts of magnetite are produced at this stage is still a matter of debate [*Bach et al*., 2006; *Evans*, 2008; *Beard et al*., 2009; *Katayama et al*., 2010]. As the system evolves toward a more fluid-dominated environment characterized by more oxidizing conditions, thicker "Type 2" veins develop that host lizardite, brucite, and magnetite. Within the Type 2 veins magnetite is formed by the extraction of iron from brucite and lizardite at the vein center, resulting in an increase of oxygen fugacity and silica activity [*Bach et al*., 2006; *Beard et al*., 2009; *Frost et al*., 2013]. Fluid-rock interaction continues at the vein edges, where new lizardite and brucite are produced from olivine.

As a result of a simultaneous decrease in density (olivine and pyroxene have densities of ~3.37 g/cm^3 and ~3.28 g/cm^3, respectively, whereas the reaction product serpentine has a density of ~2.55 g/cm^3) [*O'Hanley*, 1996], within a mass-conservative system serpentinization is typically accompanied by up to ~40% solid volume increase. Accordingly, the bulk density of unaltered peridotite (~3.3 g/cm^3) can be considerably reduced (down to ~2.6 g/cm^3) during serpentinization. *Miller and Christensen* [1997] formulated a linear, inverse correlation between density (d) and degree of serpentinization (S) according to the following equation:

$$S = (3.3 - d)/0.785 \quad (2)$$

As indicated above, serpentinization of ultramafic rocks is associated with production of magnetite, which leads to the acquisition of magnetic remanences [*Lienert and Wasilewski*, 1979; *Bina and Henry*, 1990; *Toft et al*., 1990; *Oufi et al*., 2002; *Alt et al*., 2009]. For this reason, the magnetic properties of ultramafic rocks (i.e., magnetic susceptibility (k), natural remanent magnetization (NRM), median destructive field (MDF),

hysteresis parameters (Mrs, Ms, Hcr, Hc), and grain-size and abundance of magnetite (*m*)) are strictly related to the degree of serpentinization.

Previous studies of abyssal peridotites collected at DSDP and ODP sites [*Bina and Henry*, 1990; *Toft et al*., 1990; *Kelso et al*., 1996; *Oufi et al*., 2002; *Kelemen et al*., 2004; *Bach et al*., 2004, 2006; *Paulik et al*., 2006; *Beard et al*., 2009; *Klein et al*., 2014], in conjunction with observations from ophiolites [e.g., *Coleman and Keith*, 1971; *Plümper et al*., 2012a], geochemical modeling [e.g., *Klein et al*., 2009], and experiments [e.g., *Malvoisin et al*., 2012] have allowed the geochemical and mechanical processes associated with peridotite serpentinization (and the way in which fluids migrate into, metamorphose and metasomatize the rock) to be constrained. The magnetic properties of variably serpentinized abyssal peridotites presented in a compilation of data from ocean drilling sites (most of which comprises the MAP database presented in this study) showed the existence of a direct (usually) exponential correlation between some magnetic properties (i.e., magnetic susceptibility and grain-size of magnetite) and the degree of serpentinization [*Oufi et al*., 2002]. Such correlations are, however, usually poor, and only refer to highly serpentinized samples, leaving open questions about the properties of weakly serpentinized peridotites and how they evolve during the entire serpentinization process.

3. Geology of the Sampling Area

The Mirdita ophiolite in the Albanides, part of the Hellenic-Dinaric mountain belt, is one of a major belt of ophiolites running from Slovenia to Greece that formed within a branch of the Neotethys Ocean known as the "Vardar" Ocean [*Bortolotti et al*., 1996, 2013; *Robertson and Shallo*, 2000; *Dilek et al*. 2005, 2008; *Bortolotti and Principi*, 2005; *Dilek*, 2010; *Robertson*, 2012]. Ophiolite formation initiated with intraoceanic subduction, usually interpreted to start with the formation of metamorphic soles below the Hellenic-Dinaric ophiolites in the middle Jurassic (174–160 Ma) [*Dimo-Lahitte et al*., 2001; *Liati et al*., 2004]. This was followed by emplacement of the fore-arc region of the overriding lithosphere of the Vardar Ocean onto the Adria continental margin in the Early Cretaceous (~130 Ma) [e.g., *Schmid et al*., 2008]. Subsequent to their emplacement, the Adria continental domain including the passively overlying ophiolites became involved in collision with Eurasian continental units leading to nappe stacking and rethrusting of the ophiolites during the late Cretaceous and Paleogene [*van Hinsbergen et al*., 2005; *Schmid et al*., 2008; *Toljić et al*., 2013].

Within the Western Mirdita Ophiolite, two ultramafic massifs (the Puka and Krabbi massifs) are found in tectonic, faulted contact with an upper crustal volcanic sequence (basaltic pillow lavas and dykes). This fault excises the entire lower crust (gabbros) and part of the lower upper crust (sheeted dykes), and contains amphibolite lenses, interpreted to have resulted from emplacement of a hot peridotite footwall against crustal rocks. Petrological [*Nicolas et al*., 1999], structural [*Tremblay et al*., 2009], and paleomagnetic [*Maffione et al*., 2013] evidence proves that this fault was originally an oceanic detachment that unroofed the mantle sequence (Puka and Krabbi ultramafic massifs) and resulted in the formation of an OCC. The fossil OCC (hereinafter called "the Mirdita OCC") was preserved during ophiolite emplacement onto the Adriatic continental crust and is now exposed at the surface. In this study, we analyzed a total of 144 peridotite samples collected at 14 different sites from this OCC [see *Maffione et al*., 2013, Figure 1].

4. Laboratory Techniques and Results

4.1. Serpentinization Degree

The degree of serpentinization (*S*) was computed from bulk density values using equation (2). Bulk density (*d*) of the samples was obtained from mass and volume measurements made using a high precision ($\pm 10^{-4}$ g) microbalance and a water-pycnometer, respectively. Typical densities of the Mirdita OCC peridotites are in the range of 2.63–3.29 g/cm^3 (supporting information text S1). The serpentinization degree calculated from equation (2) was corrected for the amount of newly formed magnetite, providing a corrected serpentinization degree (*Sc*) calculated from the equation of *Oufi et al*. [2002]:

$$Sc = \{3.3 - [(d - 5.2 \times m)/(1 - m)]\}/0.785 \quad (3)$$

where *m* is the magnetite volume fraction (expressed in %) given by:

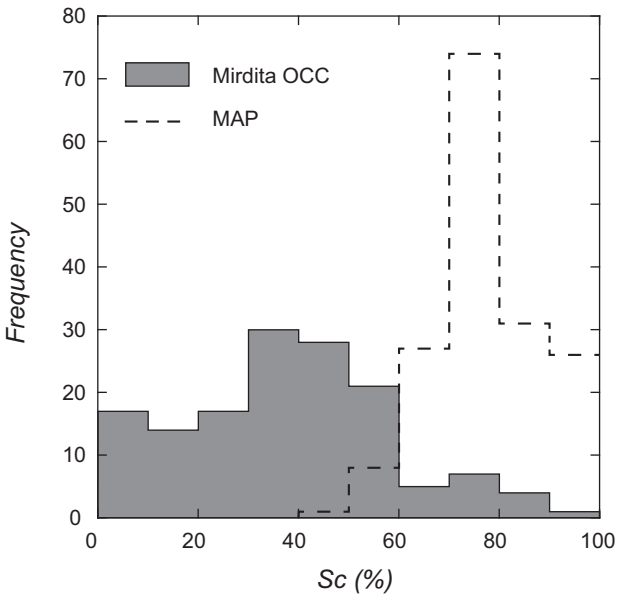

Figure 1. Frequency distribution of the degree of serpentinization (*Sc*) of 144 peridotite samples from the Mirdita OCC (this study), and 239 samples from previous DSDP/ODP sites constituting the MAP database (supporting information text S2).

$$m = (M_S)/92 \times 100 \quad (4)$$

and M_S is the saturation magnetization obtained from hysteresis experiments (see section 4.3.5.2), and 92 (Am^2/kg) is the saturation magnetization of pure magnetite.

Computed corrected serpentinization degree values from the Mirdita OCC range between 1% and 95% (Figure 1 and supporting information text S1), with most of the samples showing relatively weak degrees of serpentinization ($<\sim$60%). Corrected serpentinization degree values were also calculated for the MAP samples using equations (3) and (4). The spectra of serpentinization degrees for the Mirdita OCC and MAP samples slightly overlap (Figure 1), providing a robust data set covering the full range of serpentinization degrees.

4.2. Petrographic Characteristics

Microstructures were examined in polished thin sections using polarized light microscopy. Back-scattered electron (BSE) images were acquired using a JEOL 6610-LV (Institut für Mineralogie, University of Münster, Germany) and a FEI Nova 600 NanoLab (Electron Microscopy Center, Utrecht University, Netherlands) scanning electron microscope (SEM).

The Mirdita OCC peridotites are represented by clinopyroxene-bearing harzburgites with a local development of plagioclase-lherzolites. Nearly all thin sections ($n = 18$) display a (strong) macroscopic foliation that is reflected at the micron-scale by porphyroclastic to submylonitic textures characterized by variable amounts of dynamic recrystallization of the olivine grains (Figure 2). Only minor orthopyroxene has been identified. For a more detailed description of the olivine textures see *Nicolas et al.* [1999].

Peridotites showing $<$10% serpentinization are characterized by sparse serpentine (lizardite) veins that either follow olivine grain boundaries or cut across several olivine grains (Figure 3a). Magnetite occurs mainly as (sub)micron-sized particles dispersed throughout the veins (Figure 3b), but infrequently larger (5–10 μm) magnetite grain aggregates develop. With increasing serpentinization degree (10–40%) a typical mesh texture evolves (Figures 3c and 3d). (Sub)micron-sized magnetite grains remain commonly visible throughout the mesh texture, but larger magnetite grains develop within the vein centers. Peridotites characterized by higher serpentinization degrees (i.e., $\geq$40%) exhibit wide (400–600 μm), orthogonally cutting serpentine vein networks (Figure 3e). Large magnetite grain aggregates (100–500 μm) occur either within the vein centers (Figures 2c and 3e), displaying complex growth structures similar to dendritic crystallization patterns (Figure 3f), or are heterogeneously scattered throughout the rock (Figures 3g and h). Moreover, antigorite needles overgrowing lizardite mesh textures are commonly found in peridotites with high serpentinization degrees (Figure 3d).

4.3. Magnetic Properties of Variably Serpentinized Peridotites

4.3.1. Thermomagnetic Evidence for Presence of Magnetite

Thermal variations (both at low and high-temperatures) of low-field magnetic susceptibility were measured with an AGICO KLY-3 Kappabridge coupled to an AGICO CS3 apparatus on 18 representative samples to identify the nature of the magnetic carriers. In the low-temperature experiments, samples were cooled to $\sim$77 K using liquid nitrogen, and *k* was then continuously measured during progressive warming up to room temperature. High-temperature experiments were performed measuring *k* during a heating-cooling cycle from room temperature to 700°C in an argon atmosphere.

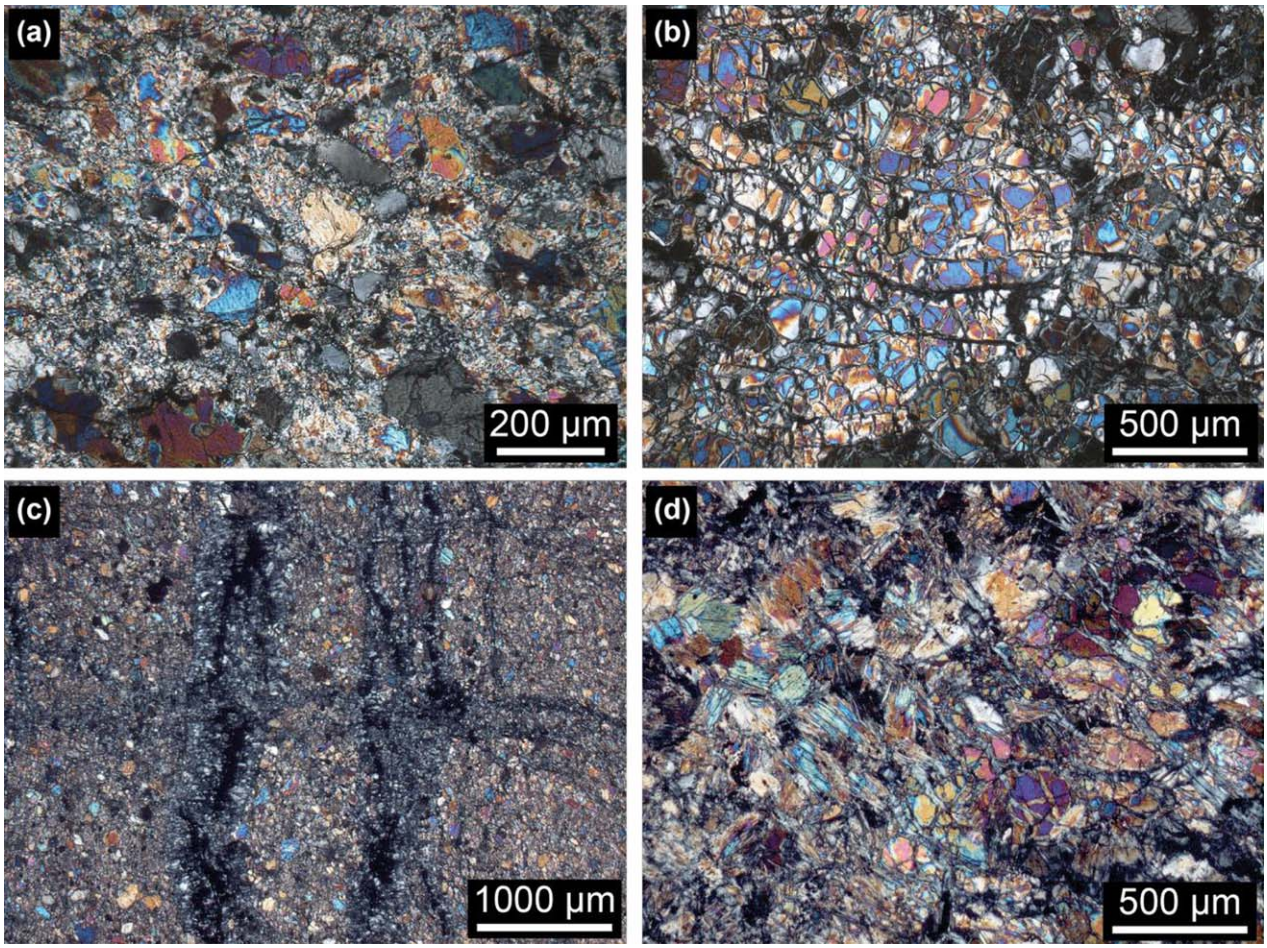

Figure 2. Optical photomicrographs under crossed polars providing an overview of varying serpentinization degrees (a) 2%, (b) 37%, (c) 46%, (d) 52% in Mirdita OCC peridotites. Olivine grains within the peridotites exhibit varying degrees of dynamic recrystallization with a development of a strong (mylonitic) fabric. Serpentinization in samples with a low alteration degree, Figures 2a and 2b, develops a typical lizardite mesh texture. Samples with a high alteration degree Figure 2c exhibit the formation of larger crosscutting serpentine veins, often filled with magnetite grains in the vein centers.

A remarkable change of k between 110 and 125 K, corresponding to the typical range of the Verwey transition in magnetite (i.e., 110–120 K) [*Özdemir et al*., 1993; *Muxworthy and McClelland*, 2000], was observed during the low-temperature experiments (Figure 4a). Almost all high-temperature experiments showed irreversible heating-cooling paths displaying the typical Curie temperature of magnetite (Figure 4b) (i.e., 578°C) [*Dunlop and Özdemir*, 1997].

4.3.2. Magnetite Content and its Variation During Serpentinization

Magnetite volume content (m) was computed using equation (4) for both the Mirdita OCC and MAP samples using saturation magnetization (M_S) measurements. The abundance of magnetite in the Mirdita OCC samples ranges between 0.1% and 7.4% (supporting information text S1), and appears to vary as an exponential function of serpentinization degree (Figure 5a). This trend show that a remarkable increase of magnetite production occurs after ~60–70% serpentinization. At a specific degree of serpentinization, however, magnetite content varies within the range of ~1%, indicating a variable production of magnetite upon serpentinization (Figure 5a). Such variability may be related to external (e.g., infiltrating fluid composition) and internal (e.g., local orthopyroxene abundance) factors controlling silica/hydrogen activity and oxygen fugacity [*Bach et al*., 2004, 2006; *Frost et al*., 2013], as well as the temperature of the hydrothermal system [e.g., *Klein et al*., 2014].

Variation of magnetite content in the MAP database mimics the exponential trend shown by the Mirdita OCC samples (Figure 5a). However, the scatter of magnetite content at a given degree of serpentinization, that was within ~1% in the Mirdita OCC data set, here seems to increase exponentially at higher degrees of

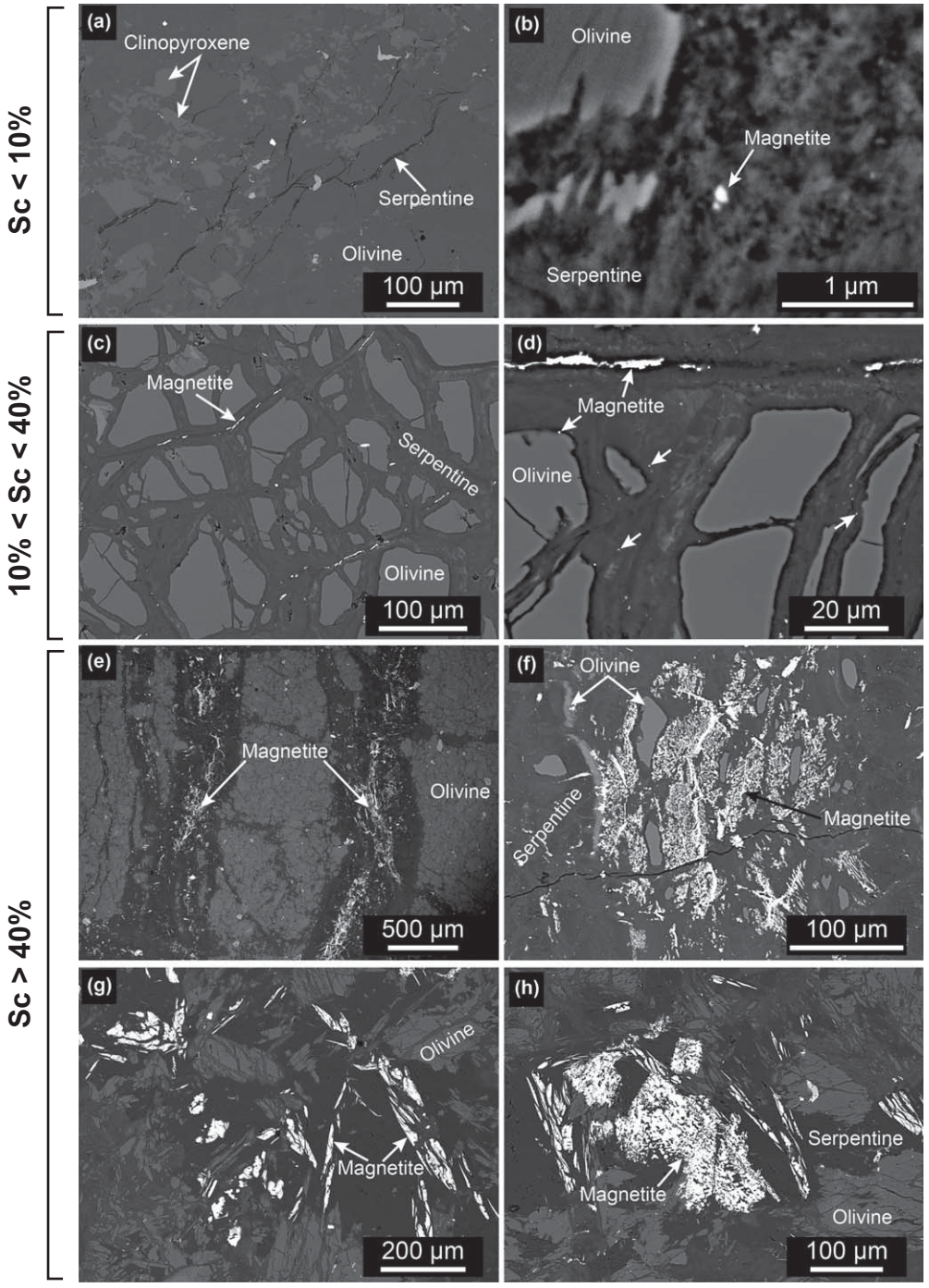

Figure 3. BSE images of serpentinized peridotites from the Mirdita OCC. The range of serpentinization degree of each group of images is shown. (a and b) Magnetite grains in samples with a very low serpentinization degree (2%) are predominantly (sub)micron in size; occasionally larger grain aggregates (5–10 µm) occur. (c and d) Magnetite grains in samples with an intermediate serpentinization degree ($10\% < Sc < 40\%$) are again mainly (sub)micron sized. However, larger grains frequently develop in the center of serpentine veins (Type 2 veins). (e–h) Samples characterized by high degrees serpentinization (>40%) display large (>50 µm), complex structured magnetite grains either (e and f) making up major parts within wide serpentine vein centers, or (g and h) heterogeneously distributed throughout the rock.

serpentinization (from ±1% to ±5% for $Sc > 60\%$). Another source of scatter, along with the composition of the reacting fluids [*Bach et al*., 2004, 2006; *Frost et al*., 2013] and local temperature [*Klein et al*., 2014], may be the variable degree of maghemitization of these samples [documented by *Oufi et al*., 2002], influencing the calculation of the magnetite content using equation (4).

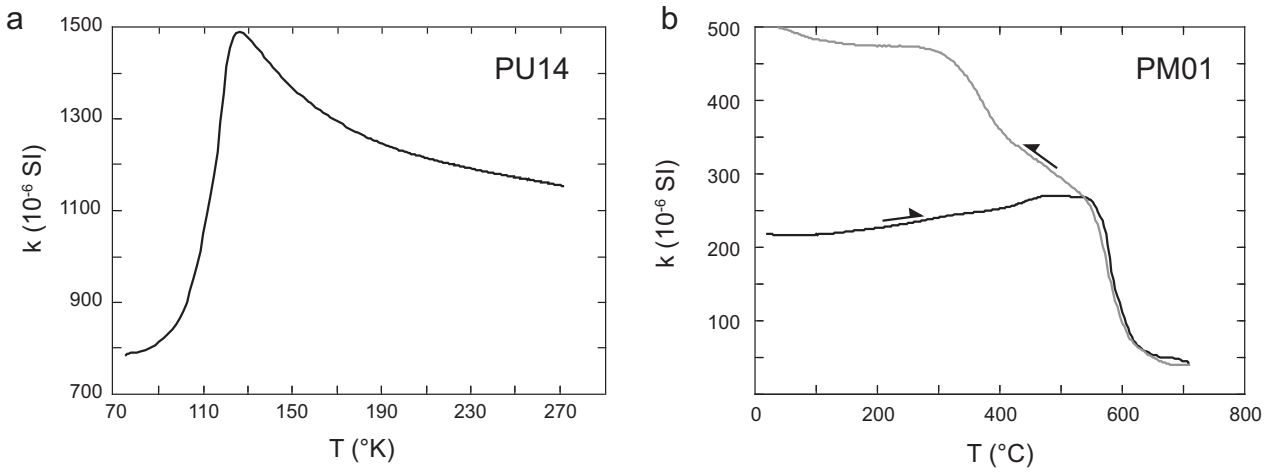

Figure 4. (a) Low-temperature thermal variation of low-field magnetic susceptibility (k) for a representative sample showing a rapid increase of k between 110 and 125 K, corresponding to the Verwey transition in magnetite. (b) Variation of k during a heating-cooling cycle (black and gray lines, respectively) from room temperature to 700°C, indicating a magnetite Curie temperature of ~580°C. CUREVAL 8.0.1 software (AGICO) was used for data analysis and graphic output.

Despite the nontrivial scatter within the combined data set (Mirdita OCC + MAP), we performed a best-fit analysis and calculated the following exponential function:

$$m = 0.23 \times \exp(0.03 \times Sc); \text{ correlation coefficient } (R) = 0.68 \quad (5)$$

The relatively high correlation coefficient indicates that this data set is well described by equation (5). However, the envelope of the distribution (i.e., maximum and minimum amounts of magnetite) and its general trend are more informative than the absolute values provided by equation (5). According to this distribution, magnetite production increases exponentially with serpentinization (with an acceleration after ~60–70% serpentinization), in agreement with previous studies [*Oufi et al.*, 2002], but in contrast to linear increments observed during hydrothermal experiments [*Malvoisin et al.*, 2012]. This evidence, combined with the significant variability of magnetite production observed in the MAP database, suggest that the local physical/chemical conditions of the hydrothermal system may have a direct control on the amount of by-products (i.e., magnetite) but not in the general timing of the serpentinization reactions (i.e., rapid acceleration at $Sc > \sim 60\%$).

4.3.3. Natural Remanent Magnetization

Standard cylindrical specimens obtained from paleomagnetic cores were exposed to a stepwise alternating field (AF) or thermal demagnetization to constrain the properties of their remanence. AF demagnetization was performed with an LDA-3A demagnetizer (AGICO), and a SQUID cryogenic magnetometer (2G Enterprises), by progressively applying 2–5 mT AF increments up to 100 mT. Thermal treatment was carried out within a magnetically shielded oven through variable (20–50°C) temperature increments up to 580°C. Magnetic remanence was measured at each demagnetization step with a JR-6A spinner magnetometer (AGICO) or a 2G SQUID cryogenic magnetometer, depending on the magnetization intensity compared to instrumental sensitivity.

Samples from the Mirdita OCC display a wide range of natural remanent magnetizations (NRM) between 0.016 and 29.3 A/m (1.61 A/m on average; supporting information text S1). NRM intensity of a rock sample is controlled by many factors, such as the type, amount, and oxidation degree of the ferromagnetic minerals, and the nature of the remanence components (i.e., coexistence of antiparallel components acquired at different times [*Schlinger*, 1985], and possible interactions between large magnetite grains). The predominant occurrence of magnetite in the Mirdita OCC samples excludes the presence of different magnetic carriers as a possible source of scattering of NRM. The overall increase of NRM with degree of serpentinization, roughly approximated by an exponential trend, indicates that the variable amount of magnetite produced during serpentinization is the main factor controlling the NRM distribution in this data set (Figure 5b). However, the range of NRM values at a specific serpentinization degree is almost two orders of magnitude.

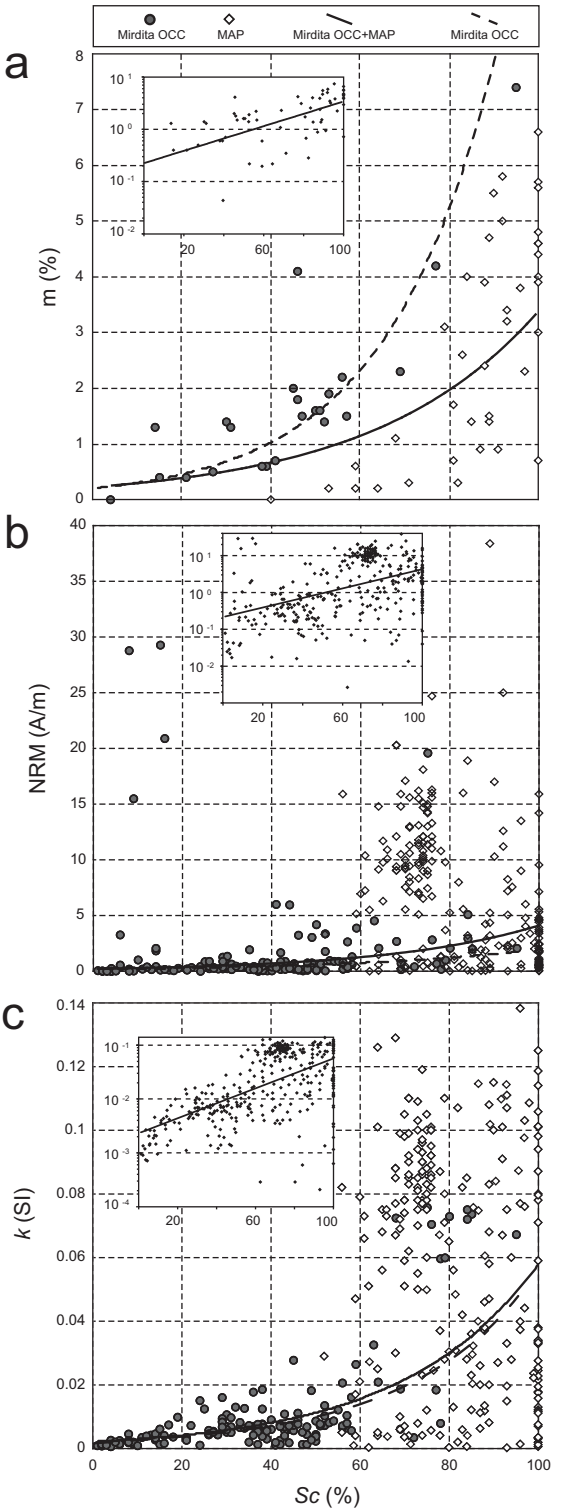

Figure 5. Variation of (a) magnetite volume content (*m*), (b) intensity of the natural remanent magnetization (NRM), and (c) magnetic susceptibility (*k*) with the degree of serpentinization (*Sc*) for the peridotites from the Mirdita OCC and MAP (see text). Separate exponential trends are calculated from both the Mirdita OCC (dotted line) and a combined (full line) data sets. Insets of Figures 5b and 5c show the same data with vertical axes on a logarithmic scale.

Weathering and low-temperature oxidation (maghemitization) [*Prévot et al*., 1981; *Özdemir*, 1990] may contribute to this scatter, and, in few specific cases (i.e., samples with extremely high NRM and low serpentinization degree), the NRM may reflect a strong isothermal remanent magnetization (IRM) likely acquired by lightning.

Similarly, the significant scatter of NRM observed in samples from the MAP database may be caused by a combination of variable amounts of magnetite and oxidation degree. In particular, drilling-induced magnetizations may significantly affect samples from the DSDP and ODP sites of the MAP data set. The variation of NRM with serpentinization in the combined data set (Mirdita OCC + MAP) is described by the following exponential function:

$$\text{NRM} = 0.22 \times \exp(0.03 \times Sc); \quad \text{correlation coefficient } (R) = 0.13 \tag{6}$$

Despite the low correlation coefficient, a general exponential trend appears to be a distinct feature of this combined data set. In particular, substantially higher NRMs showing a progressive increase can be observed after ~60% serpentinization degree. Although this effect may possibly be related to the juxtaposition of two data sets (Mirdita OCC and MAP) characterized by different local chemical conditions (the 60% threshold roughly divides the two data sets), the similarity with the distribution observed in the Mirdita OCC data set alone suggests that the rapid increase of NRM at *Sc* = ~60% is a general feature of all variably serpentinized peridotites.

4.3.4. Magnetic Susceptibility

Magnetic susceptibility (*k*) is a parameter related to the nature and concentration of ferromagnetic minerals [*Tauxe*, 2010]. Magnetite production during serpentinization, therefore, results in a significant modification of the original susceptibility. We measured the low-field magnetic susceptibility of the Mirdita OCC samples with an AGICO KLY-3 Kappabridge, with values normalized to a standard volume of 10 cm^3. Susceptibility is quite variable and ranges between 0.0007 and 0.0758 SI (0.014 SI on average; supporting information text S1), and

increases exponentially with serpentinization degree (Figure 5c), showing a four-fold increment at ~60% serpentinization where it passes from ~0.02 to ~0.08 SI.

MAP samples display a substantial scatter in susceptibility (0.0002–0.153 SI) that is only partially related to the serpentinization degree. A variable degree of maghemitization [*Oufi et al*., 2002] may have affected the original bulk susceptibility of these rocks [*Prévot et al*., 1981; *Özdemir*, 1990]. The variable amount of magnetite produced at discrete degrees of serpentinization can easily explain most of the observed scattering.

Although the scatter of susceptibility in the MAP database cannot be disregarded, the exponential trend calculated for the combined data set (Mirdita OCC + MAP) is strikingly consistent with that calculated from the Mirdita OCC data set alone (Figure 5c). A general relationship between susceptibility and serpentinization degree in variably serpentinized peridotites can therefore be described by the following equation:

$$k = 0.002 \times \exp(0.03 \times Sc);\ \text{correlation coefficient}\ (R) = 0.59 \quad (7)$$

This exponential trend indicates that magnetic susceptibility increases moderately during the early stages of serpentinization (<~60% serpentinization), remaining below ~0.02 SI. Upon ~60% serpentinization, it rapidly increases due to the increase in magnetite production shown in Figure 5a.

4.3.5. Grain-Size Variation of Magnetite

4.3.5.1. First-Order Reversal Curves (FORCs)

FORC diagrams are obtained from a suite of partial hysteresis curves called first-order reversal curves [e.g., *Mayergoyz*, 1986], and are commonly used to characterize coercivity and grain-size distributions in ferromagnetic minerals [e.g., *Roberts et al*., 2000]. FORC diagrams were calculated for 26 representative samples from the Mirdita OCC, with variable serpentinization degrees, using a Princeton Micromag vibrating sample magnetometer. A number of FORCs, varying between 36 and 111, have been processed at each sample to obtain a single FORC diagram. Most of the obtained FORC diagrams (Figure 6) show a considerable vertical spread (along the *Hu* axis), with peak distributions commonly located just below the $Hu = 0$ axis. These two features have been previously explained by the presence of interacting particles affected by a stabilizing mean interaction field [*Pike et al*., 1999; *Roberts et al*., 2000]. Most samples have FORC diagram contours closing around a peak that occurs at coercivities (*Hc* axis) between 8 and 28 mT (average: 20.3 mT; Figure 6). Closed contours and a symmetric vertical profile (along a section parallel to the *Hu* axis), are typical features of interacting single-domain (SD) grains [*Roberts et al*., 2000]. Further samples display simultaneous presence of pseudo-single-domain (PSD) and SD grains, based on the following evidence: (i) the outer contours of the FORC diagrams diverge from the intersection of the axes, whereas the inner contours are less divergent; (ii) the profile of the distribution along the *Hu* axis is slightly asymmetric; (iii) the coercivity peak occurs at lower values (average: 19.2 mT). The coexistence of SD, PSD, and multidomain (MD) fractions has also been interpreted from diagrams showing the occurrence of the features described above, together with external divergent contours typical for MD grains [*Roberts et al*., 2000]. Lastly, a small group of samples show contours forming a plateau close to the origin of the *Hc* axis, indicating the presence of superparamagnetic (SP) grains (Figure 6).

The shape of the FORC diagrams, and hence the grain size, shows a clear relationship with the degree of serpentinization. SP-type FORCs were observed in samples showing <10% serpentinization degree, whereas SD-type FORCs characterize samples with serpentinization degrees between ~10% and ~40%. Finally, SD + PSD-type and SD + PSD + MD-type FORCs are identified in samples with more than ~40% and ~60% serpentinization degrees, respectively (Figure 6).

4.3.5.2. Day Plot

A powerful tool widely used to discriminate ferromagnetic grain-size distributions in rock samples is the Day plot [e.g., *Day et al*., 1977]. It displays the remanence ratio (saturation remanent magnetization to saturation magnetization, M_{RS}/M_S) against the coercivity ratio (remanent coercive force to the ordinary coercive force, H_{CR}/H_C) obtained from hysteresis experiments. The remanence ratio of a representative group of Mirdita OCC samples varies between 0.16 and 0.48, falling within the PSD region of the Day plot (Figure 7a). Samples from the MAP database fall in the same PSD region. Altogether, data from the Mirdita OCC and MAP database are distributed along the theoretical mixing curve of magnetite [e.g., *Dunlop*, 2002], showing variable proportions of MD particles from <10% up to >80% (Figure 7a).

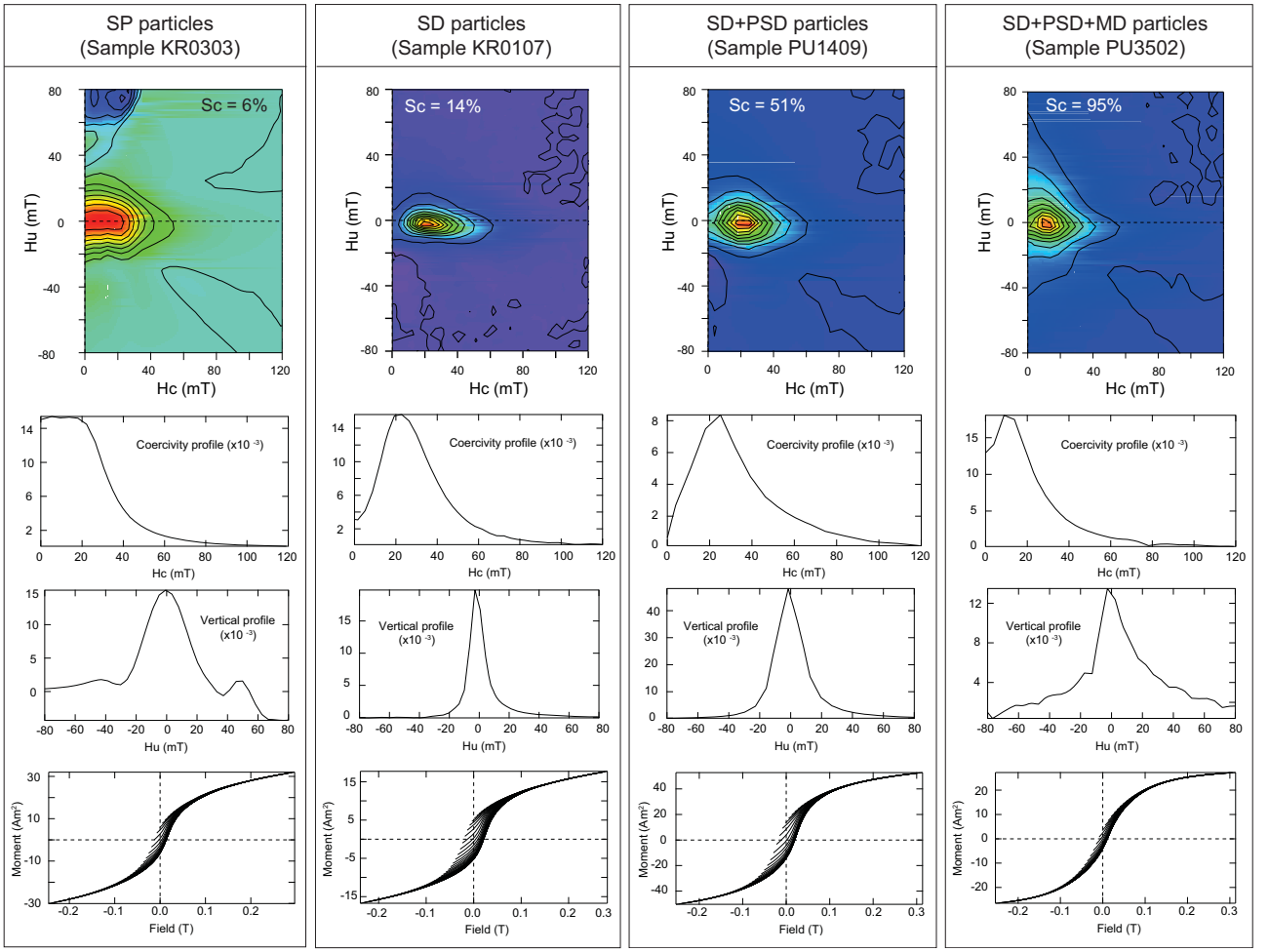

Figure 6. Results of hysteresis experiments from representative Mirdita OCC samples characterized by increasing (left to right) serpentinization degrees. From top to bottom, FORC diagrams, horizontal profiles, vertical profiles, and FORCs curves for four representative samples containing SP, SD, PSD, and MD particles in different proportions. A clear progression of grain size can be observed at increasing serpentinization degrees. FORCs were analyzed using FORCinel software [*Harrison and Feinberg*, 2008].

The remanence ratio of samples from the Mirdita OCC, which is reflective of the bulk grain-size of ferromagnetic minerals (or the amount of MD grains in a SD-MD mixture) [*Dunlop*, 2002], shows a moderate correlation with the degree of serpentinization (Figure 7b), implying that the grain size (or MD proportion) of the newly formed magnetite increases progressively during serpentinization. MAP data match well with the best-fit curve calculated for the Mirdita OCC data set. A best-fit analysis based on the combined data set (Mirdita OCC + MAP) provides a polynomial function (comparable to the one based on the Mirdita OCC data set only) characterized by a statistically significant correlation coefficient:

$$M_{RS}/M_S = -0.00002 \times Sc^2 - 0.0014 \times Sc + 0.42;\ \text{correlation coefficient}\ (R) = 0.79 \qquad (8)$$

This trend is indicative of an exponential-type growth of MD magnetite, which becomes predominant after 60–70% serpentinization.

4.3.5.3. Median Destructive Field

Median destructive field (MDF) is the magnitude of the alternating field (AF) needed to demagnetize half of the initial NRM of the sample and is a parameter dependent on the bulk coercivity (*Hc*) of the rock. In turn, *Hc* is strictly related to the grain size and nature of the magnetic carriers as well as the magnetization stability. MDF values in the Mirdita OCC samples are variable between 3 and 28 mT (average: 12.5 mT; Figure 8a), indicating the presence of a low-to-medium coercivity fraction with values typical of magnetite [*Dunlop and Özdemir*, 1997]. As magnetite is the only magnetic carrier in those rocks, the MDF is an inverse proxy for

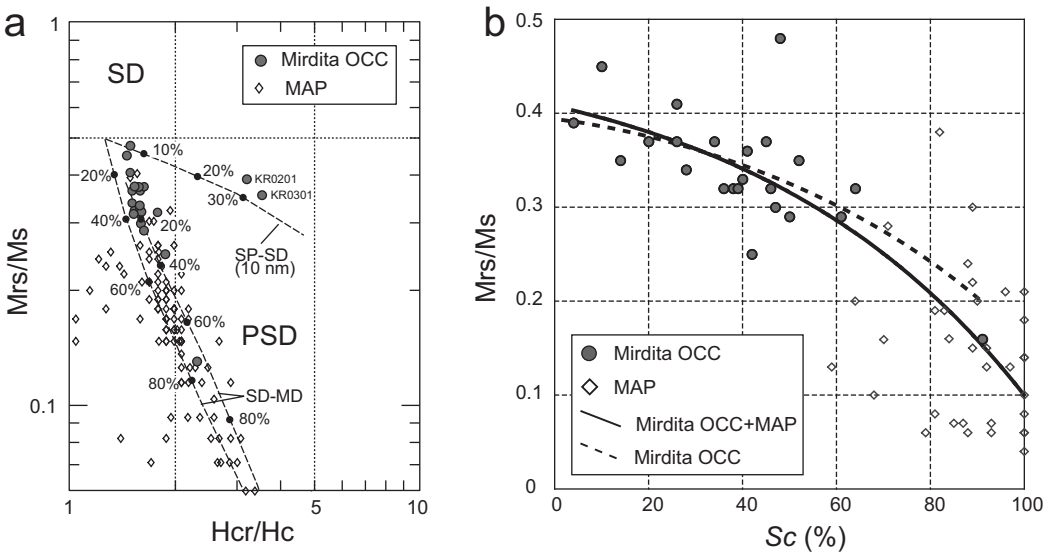

Figure 7. (a) Day plot [*Day et al.*, 1977] for 21 representative samples from the Mirdita OCC and MAP (see text). Most of the samples follow the theoretical mixing curves SD-MD for magnetite (dashed lines) of *Dunlop* [2002], showing a variable proportion of MD particles from <10% up to ~80%. Two samples are aligned along the SD-SP mixing curve and contain up to 30% SP grains. (b) Remanence ratio (Mrs/Ms) against the degree of serpentinization (Sc) for the same combined data set. Both best-fit curves for the Mirdita OCC (dotted line) and combined data sets (full line) are described by second-order polynomial functions.

magnetic grain size, and indicates the presence of SD (>20 mT), PSD (10–20 mT), and MD (<10 mT) grains. A sharp decrease in MDF is seen between ~40% and 60% serpentinization (Figure 8b), where it reduces by 50% (from ~30 to ~15 mT), reflecting a bulk grain size increase within this interval. While both SD and MD fractions are present in samples with $Sc < 40\%$, the MD fraction seems to dominate in highly serpentinized samples ($Sc > \sim 60\%$).

4.4. Remanence Characteristics and Timing of Serpentinization

Demagnetization experiments on Mirdita OCC peridotites revealed the common presence of two magnetization components (Figure 9a). A low stability component carried by MD magnetite grains was removed by alternating fields <14 mT, or at moderate to high temperatures (up to 565°C). Although this component is

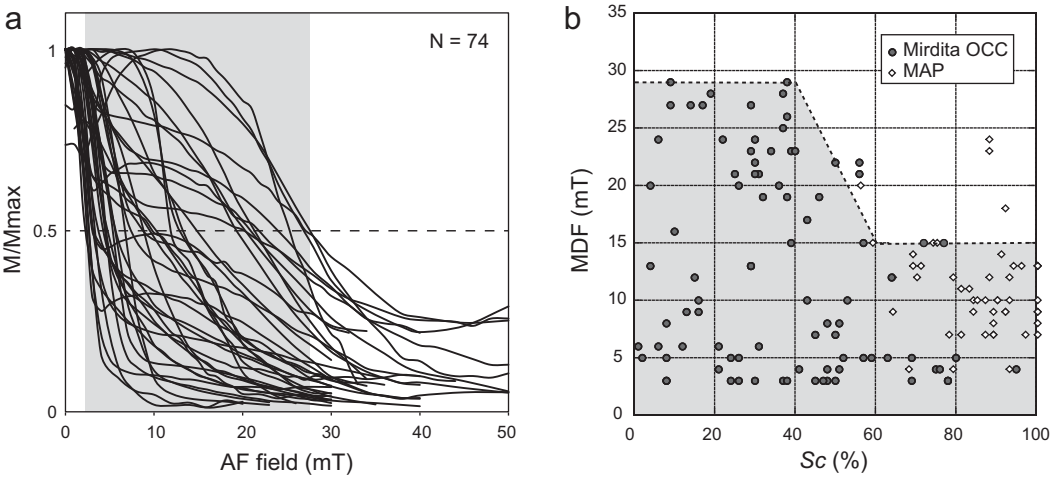

Figure 8. (a) Normalized decay curves of magnetization (M/M_{max}) during AF demagnetization of a representative group of samples from the Mirdita OCC (this study). Median destructive field (MDF) of each sample is given by the intersection between the demagnetization curve and the dashed line crossing the M/M_{max} axis at 0.5. The range of MDF for this data set is marked by the gray area. (b) Relationship between MDF and serpentinization degree (Sc) for representative samples from the Mirdita OCC and MAP. The envelope of MDF variation is highlighted by the shaded gray area showing a rapid decrease between ~40% and ~60% serpentinization degree.

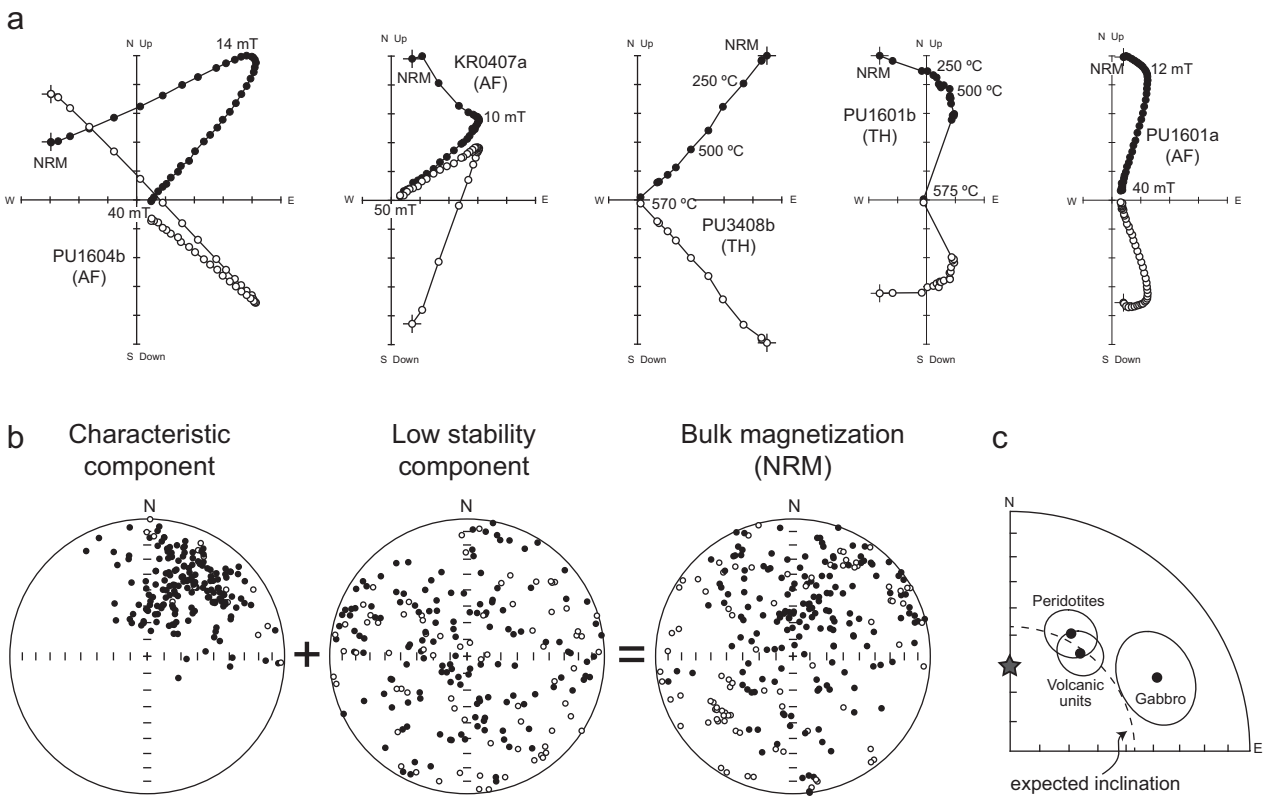

Figure 9. (a) Zijderveld diagrams [*Zijderveld*, 1967] of representative samples demagnetized using both thermal (TH) and alternating field (AF) treatment (in situ coordinates). Solid and open dots represent projections on the horizontal and vertical planes, respectively. Demagnetization step values are in °C or in mT. Magnetic component analysis and graphic output were carried out with REMASOFT 3.0 software [*Chadima and Hrouda*, 2006]. (b) Lower hemisphere stereographic projections showing the *in situ* directions of the characteristic (ChRM) component, low stability component, and NRM. (c) Mean paleomagnetic directions and associated α_{95} cones of confidence for the peridotite, volcanic, and gabbro samples from the Mirdita OCC [see *Maffione et al*., 2013, for more details]. Gray star is the present field direction expected at the sampling locality. Dotted circle is the expected inclination calculated for the Jurassic (170 Ma) reference paleopole of *Besse and Courtillot* [2002].

well defined within individual samples, its direction is scattered at both site and regional-level (Figure 9b) and does not reflect a present magnetic field overprint, a drilling-induced magnetization, or an effect of any local/regional tectonics. With each sample the maximum axes of anisotropy of magnetic susceptibility (AMS) and anisotropy of anhysteretic remanence magnetization (AARM) are not related to the NRM direction, excluding also the influence of anisotropy as a source of scatter. The random directions of the low stability components are instead best explained by either microscopic magnetic interactions between MD magnetite grains occurring within major serpentine veins, or small-scale deformation accommodated along major veins (that are mainly dominated by MD magnetite grains).

In contrast, characteristic (ChRM) remanence components are clustered at both site and regional-level (Figure 9b) and have a NE direction that is significantly different from the present geomagnetic field direction. High coercivities (15–50 mT) indicate that ChRMs are carried by stable SD and PSD magnetite grains. The mean remanence direction of the peridotites is statistically indistinguishable from that of coeval volcanic units in the detachment hanging wall (Figure 9c). Both have inclinations consistent with that expected from the Jurassic (170 Ma) European reference paleopole of *Besse and Courtillot* [2002] (dashed small circle in Figure 9c). In contrast, the mean ENE-directed remanence of gabbros intruded into the footwall peridotites is statistically different (Figure 9c) and records tectonic rotation of the footwall around a ridge-parallel axis [*Maffione et al*., 2013]. Since this rotation must also have affected the host peridotites, the remanence data are consistent with the following sequence of events: (i) acquisition of thermoremanent magnetizations by hanging wall upper crustal rocks and footwall gabbros; (ii) footwall rotation during detachment fault activity and OCC formation; and (iii) postrotation serpentinization of footwall peridotites (but not of the intruding gabbros), with acquisition of a remanence in the same direction as unrotated upper crustal rocks in the detachment hanging wall [see *Maffione et al*., 2013, for further details). The paleomagnetic data hence

indicate that serpentinization-related remanence acquisition was coeval with Jurassic seafloor spreading, and exclude serpentinization during or after ophiolite emplacement onto the Adriatic continental margin.

5. Discussion

Our integrated petrological, paleomagnetic, and rock magnetic analyses of peridotites from a fossil OCC in the Mirdita ophiolite shed light on the previously poorly constrained magnetic properties of weakly serpentinized peridotites. In combination with existing data from more highly serpentinized abyssal peridotites (MAP), they provide a complete characterization of the magnetic properties across the full spectrum of serpentinization in ultramafic rocks.

The presence of magnetite in the Mirdita OCC peridotites is confirmed by multiple lines of evidence, including: petrographic observations of thin sections (Figures 2 and 3); Verwey transition in low-temperature thermomagnetic curves (Figure 4a); Curie temperatures observed in both high-temperature thermomagnetic curves and demagnetization experiments (Figures 4b and 9a); FORC diagrams and median destructive fields (MDF) (Figures 6 and 8b); coercivity spectra from AF demagnetization (Figure 8a); and hysteresis parameters in a Day plot (Figure 7a). Low-temperature serpentinization, inferred from the predominant occurrence of lizardite, is the main mechanism responsible for the formation of magnetite in those samples, according to equation (1). Although we cannot fully exclude the occurrence of weathering and/or low-temperature oxidation of magnetite (maghemitization) [e.g., *Prévot et al*., 1981; *Özdemir*, 1990], remanence relationships (section 4.4) indicate that the magnetic properties of these peridotites result from seafloor processes. Furthermore, we exclude extensive metamorphism as the Mirdita ophiolite did not experience burial by nappe stacking during regional tectonics (being at the top of the tectonic pile of the Dinarides fold-thrust belt) [*Bortolotti et al*., 1996; *Robertson*, 2012], and escaped the major Tertiary deformation phase of the Dinarides (as suggested by subhorizontal limestones laying above the ophiolite) [*Bortolotti et al*. 1996; *Robertson and Shallo*, 2000; *Dilek*, 2010; *Meshi et al*., 2010; *Robertson*, 2012].

5.1. Progress of Serpentinization Reactions as Inferred From the Variation of Magnetic Parameters

Recent advances in geochemical and petrological studies of abyssal peridotites have revealed that serpentinization develops via multistage reactions controlled by a variety of factors, such as: silica activity; oxygen fugacity; permeability of the system (rock-dominated versus fluid-dominated); and temperature [*Bach et al*., 2006; *Frost and Beard*, 2007; *Beard et al*., 2009; *Malvoisin et al*., 2012; *Frost et al*., 2013; *Klein et al*., 2014]. This is also demonstrated by the formation of multiple sets of crosscutting veins with different mineralogies and structure [*Andreani et al*., 2007; *Frost et al*., 2013].

Early studies of serpentinized abyssal peridotites documented a possible correlation between magnetic parameters and the degree of serpentinization as a result of magnetite production [*Linert and Wasilewski*, 1979; *Toft et al*., 1990; *Bina and Henry*, 1990]. These hypotheses were later supported by a wealth of data from abyssal peridotites collected at several oceanic drill sites [*Oufi et al*., 2002; *Kelemen et al*., 2004; *Alt et al*., 2009], and presented in this study as a new database (MAP; supporting information text S2). Although it is now widely accepted that serpentinization is one of the main processes responsible for magnetite production in ultramafic rocks, the rate at which magnetite forms during hydrothermal activity is still unclear. A variety of models have been put forward to explain variations in magnetic parameters due to serpentinization. *Toft et al*. [1990] attributed the exponential increase of susceptibility to a progressive acceleration in magnetite production starting after ~50% serpentinization upon breakdown of iron-rich serpentine (lizardite) and brucite into iron-poor serpentine and magnetite. More recent models [*Bach et al*., 2006; *Frost et al*., 2013] attributed this exponential increase in susceptibility solely to the breakdown of iron-rich brucite triggered by either an increase in silica activity related to the contribution of orthopyroxenes to the reactions [e.g., *Bach et al*., 2006], or the switch from rock-dominated to fluid-dominated conditions where the redox budget increases over time [e.g., *Frost et al*., 2013]. In contrast to studies from natural serpentinized peridotites, hydrothermal experiments on synthetic olivine [*Malvoisin et al*., 2012] have shown that both susceptibility and magnetite production increase linearly during serpentinization as a result of temperature and hydrogen activity variation.

Our rock magnetic results from the Mirdita OCC peridotites are consistent with previous data from mid-ocean ridge-related abyssal serpentinites, and show the existence of an exponential correlation between magnetic properties (magnetite content, NRM, and magnetic susceptibility) and serpentinization degree

(Figure 5). Serpentinization, therefore, appears to advance differently in natural settings (i.e., at mid-ocean ridges) than in laboratory experiments. In particular, the exponential increase in magnetite content (*m*) with the serpentinization degree (Figure 5a) is directly reflected in the variation of NRM (Figure 5b) and susceptibility (Figure 5c). While, the variability of *m* at a specific degree of serpentinization (i.e., the scatter on the *y* axis) is limited, within the range of ~1%, that of the NRM and *k* is much more substantial (within one or two orders of magnitude) (Figure 5), and likely related to a variable degree of weathering and maghemitization of the original magnetite [*Prévot et al*., 1981].

For each magnetic parameter, data from the MAP database are mostly consistent with the exponential trends described by the Mirdita OCC samples (Figure 5). Best-fit curves calculated for the combined data set (Mirdita OCC + MAP) are, in fact, comparable to those computed from the Mirdita OCC data alone. The significant scatter of parameters in the MAP database, affecting the results of the best-fit analyses, is partly attributed to the same process responsible for the scatter observed in the Mirdita OCC samples (i.e., maghemitization and variable magnetite content). Site-to-site variability of (i) the composition of the host rock and reacting fluids, which determines the silica activity and oxygen fugacity of the system [*Bach et al*., 2004, 2006; *Frost et al*., 2013], and (ii) the temperature of the hydrothermal system [*Klein et al*., 2014] may, however, explain the more substantial variation of magnetite content (at a specific serpentinization degree) observed in the MAP database (±5%; Figure 5a). In turn, the high variability of magnetite production affects the distribution of NRM and magnetic susceptibility and their scatter (Figures 5b and c).

Despite the scatter in the combined magnetic data set (Mirdita OCC + MAP), analysis of rocks exposed to variable, local physical/chemical conditions provides insights into the permissible range of variability of magnetite content (0–7%), NRM (0.002–38.4 A/m), and magnetic susceptibility (0.0002–0.153 SI) in serpentinized abyssal peridotites (Figure 5 and supporting information text S1 and text S2).

Since both NRM and susceptibility are mainly dependent on magnetite content, their rapid increase at ~60% serpentinization must reflect an acceleration in magnetite production rate. We suggest that this is a direct result of the transition from a rock-dominated to a fluid-dominated system [*Frost et al*., 2013]. The establishment of an open circulation of fluids in the rock body may be related to a dramatic increase in transient permeability due to pervasive reaction-induced mechanical weakening at a critical serpentinization threshold of about 60%. This transition might explain the discrepancy between the evolution of magnetic properties in synthetic and natural serpentinized peridotites (linear [*Malvoisin et al*., 2012] versus exponential variations, respectively). In addition, the paucity (or total lack) of orthopyroxene in the Mirdita OCC peridotites excludes, in this specific case, the effect of orthopyroxene alteration [*Bach et al*., 2006] as a possible mechanism for the exponential increase of magnetite production during serpentinization.

Based on the above discussion, we propose the following alternative model for magnetite production during serpentinization. During the initial phases of hydrothermal activity (<~60% serpentinization), magnetite forms within thin, sparse veins, whose number and thickness increase as the reactions progress. At ~60% serpentinization a pervasive mechanical breaking of the rock occurs due to the internal solid volume increase [e.g., *Plümper et al*., 2012b], and new fresh surfaces of olivine are exposed to alteration along major veins. The system changes from rock-dominated to fluid-dominated, drastically increasing the redox budget. Iron-rich brucite formed at the vein center reacts to produce magnetite and hydrogen.

It is worth noting that both BSE images (Figure 3) and rock magnetic analyses (Figure 5a) document the presence of magnetite also in extremely fresh peridotites ($Sc < 10\%$). This evidence implies that small amounts of magnetite may form during the incipient phases of serpentinization, in agreement with *Evans* [2008] but in contrast with other models that neglect magnetite production at the onset of reaction [*Bach et al*., 2006; *Frost and Beard*, 2007; *Beard et al*., 2009; *Frost et al*., 2013].

Although the relationship between the degree of serpentinization and magnetite grain size has been investigated in several studies, no clear correlation between the two parameters has been identified so far [*Bina and Henry*, 1990; *Oufi et al*., 2002]. The investigation of magnetite grain size during serpentinization in our combined data set using four independent techniques (Figures 2, 3, 6–8), now provides a clearer view of the grain-size evolution of magnetite.

Bina and Henry [1990] proposed that smaller magnetic grains form during the early stages of serpentinization, yielding a weak but stable magnetization, and that larger particles are generated at subsequent stages.

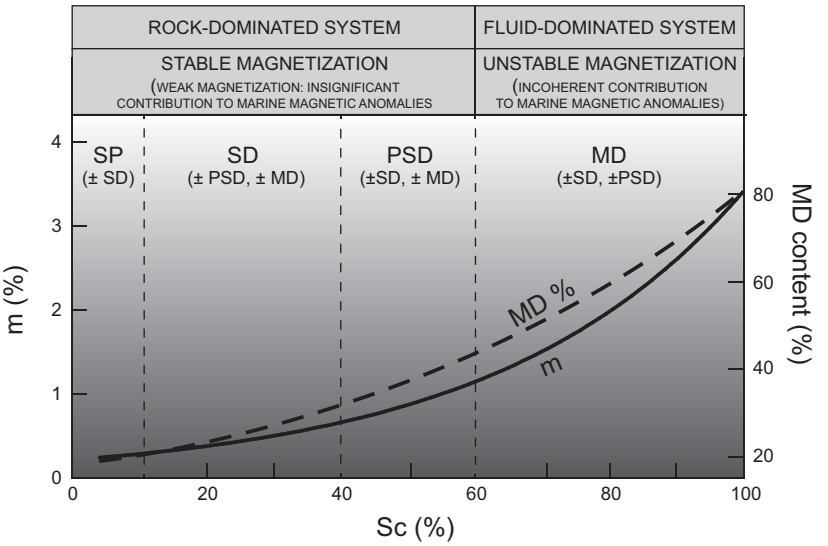

Figure 10. Summary diagram showing the effect of serpentinization on the magnetic properties and remanence of the Mirdita OCC peridotites. Both the volume content (*m*) and grain size (% MD/PSD fraction) of magnetite increase in an exponential fashion during serpentinization. Larger magnetite grains progressively form during serpentinization reactions: SD, PSD, and MD grains grow as a dominating phase at ~10%, 40%, and 60% reaction progress, respectively. Above ~60% serpentinization the system moves from rock to fluid-dominated, resulting in exponential increases of magnetite production, grain size, and magnetic susceptibility. The MD fraction formed after ~60% serpentinization adversely affects the directional stability of the magnetic remanence. SP, super-paramagnetic; SD, single-domain; PSD, pseudo-single-domain; MD, multidomain.

In contrast, *Malvoisin et al.* [2012] documented the formation of MD magnetite (1–20 μm) at all stages of their experiments. Overall, our results from the Mirdita OCC are consistent with the conclusions of *Bina and Henry* [1990], although sparse MD grains have been observed also in thin sections from weakly serpentinized samples (Figures 3a and 3b). A more detailed evolution of magnetite grain size during serpentinization, however, can be estimated by combining the results from the different analyses. FORC diagrams (Figure 6) document the occurrence of SP, SD, PSD, and MD grains in different proportions as a function of the serpentinization degree, in agreement with observations in thin sections (Figure 2), BSE images (Figure 3), and the MDF distribution (Figure 8). Furthermore, the content of MD magnetite increases exponentially during serpentinization (Figure 7b).

A summary diagram showing the evolution of the amount and grain size of magnetite produced during serpentinization is presented in Figure 10. SP ($<<$0.05 μm), and minor SD ($<$0.05 μm) magnetite particles are produced during the initial stages of serpentinization (i.e., *Sc* $<$10%). With ongoing reactions (*Sc* $>$ 10%) mainly SD and minor PSD (0.05–3 μm) and MD ($>$3 μm) grains grow, followed by a more substantial production of PSD grains (and minor MD) at ~40% serpentinization, and finally mainly MD particles after ~60% serpentinization. This is in agreement with SEM observations (Figure 3) that reveal a dominance of (sub)micron-sized magnetite grains and only sparse larger (MD) grains in peridotites with a low serpentinization degree, whereas truly MD magnetite grain aggregates hosted by larger serpentine veins dominate in peridotites with high serpentinization degrees. The presence of SD grains in samples characterized by low serpentinization degrees (i.e., $<$10%), in agreement with *Evans* [2008], is also indicated by their stable remanence that cannot be carried by the SP fraction only.

The largest MD magnetite grains, hosted by large serpentine veins, appear to grow mainly after ~60% serpentinization, in response to the rapid increase in the magnetite production rate resulting from the change from rock to fluid-dominated conditions (Figure 10). In turn, this effect has profound implications for the nature and stability of the magnetic remanence (see next section).

5.2. Implications for the Origin of Marine Magnetic Anomalies

Fresh peridotites are not remanence-bearing due to the presence of only paramagnetic minerals, so the development of stable magnetic remanences in marine environments can only be achieved by serpentinization [*Toft et al.*, 1990; *Bina and Henry*, 1990; *Oufi et al.*, 2002; *Gee and Kent*, 2007; this study].

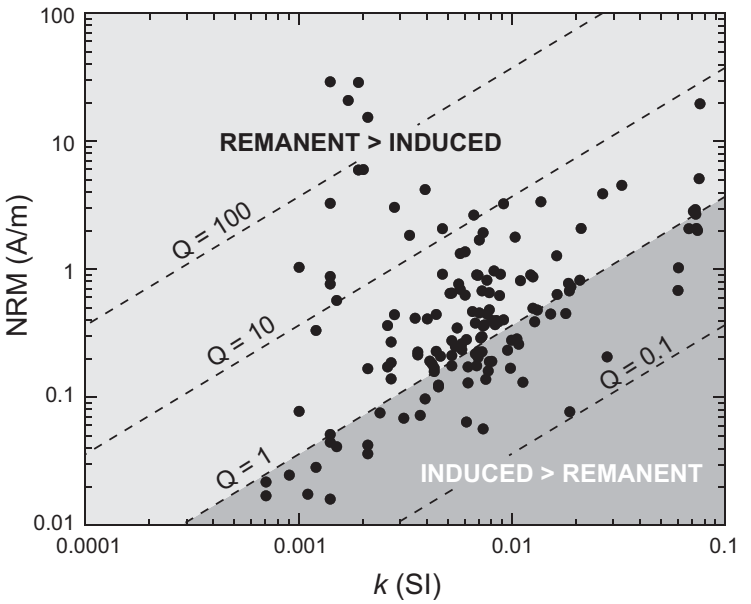

Figure 11. Log-log plot of NRM and susceptibility of oceanic serpentinized peridotite samples from the Mirdita OCC compared to lines of constant Q (Königsberger ratio) calculated for field of 37.2 A/m. Only 65% of samples (light gray shaded area) are potentially able to contribute to oceanic magnetic anomalies (i.e., have remanence greater than induced magnetization: $Q > 1.0$). Thirty-five percent of samples have $Q < 1.0$ (induced magnetization greater than remanence; dark gray shaded area) and would not be effective as a source for oceanic magnetic anomalies.

Hysteresis experiments indicated that SD magnetite grains are present in variable amounts in all samples, and that they mainly formed during the initial stages (10–40%) of serpentinization (Figure 10). PSD magnetite is potentially formed together with SD grains, although FORC analysis provides clear evidence for presence of PSD grains only after ~40% serpentinization. The presence of a stable remanence in the freshest samples (<10% serpentinization), that rock magnetically are dominated by a (nonremanence-carrying) SP magnetic fraction, implies presence of SD magnetite even at the earliest stages of serpentinization. Since stable remanences are commonly carried by SD and small PSD grains, we conclude that a coherent, high-stability remanence is only acquired during the initial stages of serpentinization ($Sc < \sim 60\%$).

Placing our results (Figure 10) in the context of the model proposed by *Frost et al*. [2013], we argue that the most stable (ChRM) magnetic remanence in serpentinized oceanic peridotites is exclusively carried by SD and PSD magnetite within pervasive, thin Type 1 veins (50–100 μm wide) formed during the initial, rock-dominated phase of the system (<~60% serpentinization). Upon substantial serpentinization-induced cracking of the rock (>~60% serpentinization), the system become fluid-dominated, and sparse, thicker serpentine Type 2 and Type 3 veins, dominated by MD magnetite carrying an unstable, randomly oriented remanence, develop.

In regions, where serpentinized peridotites are exposed on the seafloor, their potential contribution to marine magnetic anomalies is not controlled simply by NRM intensity, but by an interplay of factors that include the regional coherence of the NRM signal, the timing of remanence acquisition and the relative importance of remanent and induced magnetizations [*Gee and Kent*, 2007]. The average magnetization of weakly serpentinized (<40–60%) peridotites is too low (Figure 5b) to extensively contribute to the marine magnetic anomalies [*Oufi et al*., 2002]. More serpentinized (>~60%) peridotites have higher NRM intensities, but are affected by randomly oriented, low stability components that result in incoherent NRM directions at both the site and regional scales (Figure 9b), even though consistent characteristic magnetizations can be separated by laboratory demagnetization (Figure 9b). In addition, variations in Königsberger ratio between individual samples (Figure 11), with 35% of samples having $Q < 1.0$, indicate that the anomaly signal from these rocks when exposed on the seafloor would have been variably due to remanent and induced magnetizations, again at a range of scales, further reducing the coherence of the magnetic source. Although the Königsberger ratios (Q) from the MAP database show that remanence is greater than induced magnetization, implying that those rocks constitute a potential significant source for marine magnetic anomalies, we have no information about the direction of their magnetization, and hence their coherence at a regional scale. Therefore, relying on both the Königsberger ratio and paleomagnetic directions from the Mirdita OCC, we conclude that variably serpentinized peridotites are unlikely to provide a signal capable of contributing to regionally coherent patterns of marine magnetic anomalies.

5.3. Revised Model for the Evolution of Serpentinization-Related Magnetizations at Oceanic Core Complexes (OCC)

The most common mechanism to explain the extensive exposures of upper mantle peridotites at the seafloor is detachment faulting and OCC formation [*Cann et al*., 1997; *Escartín et al*., 2008]. However, the spatial and temporal evolution of serpentinization during OCC evolution has received only minor attention since the discovery of the first structures in the mid 1990s. Two studies from the Atlantis Massif [*Boschi et al*., 2006] and the Kane transform fault [*Andreani et al*., 2007] along the MAR showed that serpentinization initiates at the detachment fault, perhaps at depths of up to ~8 km, and progressively extends into the footwall for a maximum distance of ~1 km from the fault surface. Furthermore, according to *Andreani et al*. [2007] fluid migration and serpentinization of the detachment footwall results in the generation of crosscutting serpentine veins at discrete stages of the OCC evolution. The maximum depth of ~8 km for fluid influx proposed by *Boschi et al*. [2006] and *Andreani et al*. [2007] is within the maximum theoretical limit of ~10 km at which the geostatic pressure exceeds the crystallization pressure resulting from (and required by) serpentinization [*Kelemen and Hirth*, 2012; *Plümper et al*., 2012b].

The coexistence of multiple sets of crosscutting veins in serpentinized peridotites shows that serpentinization is a multistage process [*Bach et al*., 2006; *Boschi et al*., 2006; *Frost and Beard*, 2007; *Andreani et al*., 2007; *Beard et al*., 2009; *Frost et al*., 2013; this study]. In particular, *Andreani et al*. [2007] argued that serpentinization in the MARK area (Kane transform fault, 23°N) started along the main detachment fault at 3–4 km depth (possibly up to 8 km), and then continued at shallower levels during footwall uplift. If this is true, for the case of OCCs characterized by footwall "rolling-hinge" rotation and uplift [*Buck*, 1988; *Lavier et al*., 1999; *Garcés and Gee*, 2007; *Morris et al*., 2009; *MacLeod et al*., 2011] we would expect to find different remanence directions associated with each discrete set of serpentine veins. In practice, however, this has not been observed in this study. In the serpentinized peridotites of the Mirdita OCC, the ChRMs are consistent at both the site and regional-level and indicate no footwall rotation, whereas low stability components of magnetization associated with the growth of late-stage MD magnetite grains have random (geologically meaningless) directions likely resulting from local magnetic interaction (Figure 9b). In several serpentinized peridotites recovered from OCCs associated with the Fifteen-Twenty Fracture Zone along the MAR (ODP Leg 209) [*Garcés and Gee*, 2007], single, high stability components parallel to the present geomagnetic field direction were found, with any low stability components of potential geological significance likely affected by a drilling-induced magnetic overprint. In contrast, samples recovered from the 15°45′N OCC at the MAR by high-speed wireline diamond drilling using the BRIDGE drill [*MacLeod et al*., 2002, 2011] show single components of magnetization recording substantial footwall rotation [*MacLeod et al*., 2011]. Our new data combined with previous results from Atlantic OCCs strongly suggest that stable remanences (carried by fine-grained SD magnetite) in serpentinized peridotites can be acquired at different stages of footwall unroofing and rotation. In the Mirdita OCC, remanences in serpentinized peridotites postdate those of gabbroic bodies that they host [*Maffione et al*., 2013]. These unaltered gabbros from the detachment footwall record ca. 45° rotation relative to the hanging wall, whereas the peridotite host has a magnetization indistinguishable from unrotated rocks in the detachment hanging wall [*Maffione et al*., 2013] (Figure 9c), indicating that it was acquired after footwall rotation. Variable directions of the remanence in peridotites from the Fifteen-Twenty Fracture Zone [*Garcés and Gee*, 2007] indicate a variable timing of serpentinization and remanence acquisition relative to footwall rotation. On the other hand, serpentinized peridotites sampled at the 15°45′N OCC [*MacLeod et al*., 2011] hold remanences that predate footwall rotation. Notably, these latter samples were collected from short (<1 m) cores drilled into the OCC detachment fault surface.

These observations from modern and fossil OCCs [*Andreani et al*., 2007; *Garcés and Gee*, 2007; *MacLeod et al*., 2011; this study] can be combined in the following unifying model for the magnetization of peridotites at OCCs characterized by rolling-hinge mechanisms (Figure 12). Pervasive serpentinization of upper mantle peridotites initially occurs along the developing detachment fault upon seawater penetration at depth [e.g., *Andreani et al*., 2007]. The progress and depth of serpentinization reactions in this initial stage are strongly dependent on the local thermal state of the fault. A basic requirement for serpentinization to start is that the temperature does not exceed ~400°C, although different minerals (i.e., talc) can form at higher temperatures [*Boschi et al*., 2006]. In situ upper mantle peridotites (>6 km depth) can be within the temperature range of serpentinization if (i) there is a significant cooling effect yielded by the influx of

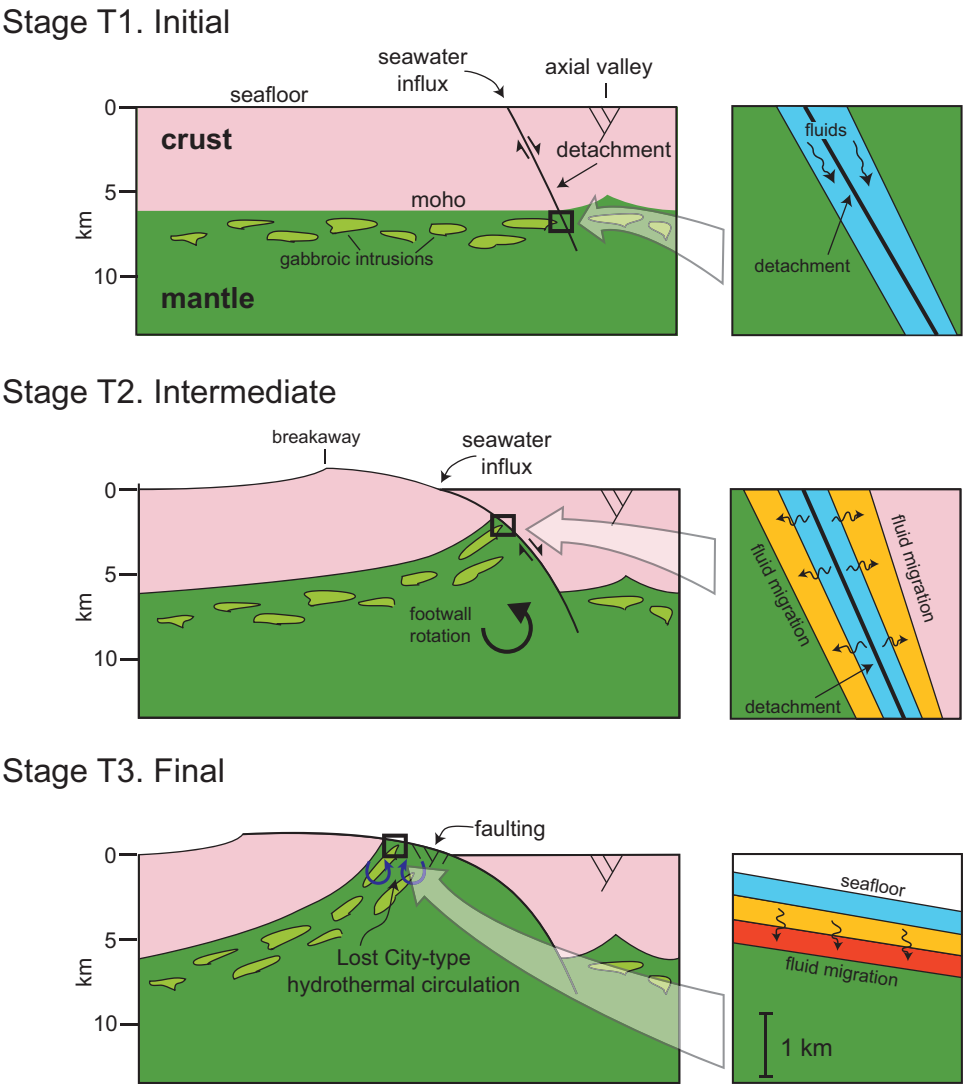

Figure 12. Evolutionary model of serpentinization during oceanic detachment faulting. At each phase (T1, T2, and T3), successively deeper portions of the detachment footwall are affected by serpentinization. The age of magnetization acquisition decreases away from the fault surface. In this model, magnetizations acquired during the earliest stage (T1) of serpentinization (blue zone) record the full history of footwall rotation, whereas magnetizations acquired upon migration of the serpentinization front into the footwall during OCC evolution (orange zone; stage T2) may record only partial rotation. Finally, magnetizations acquired by the deeper portions of the footwall (red zone) after complete rotation and uplift (stage T3) record no rotation.

seawater into the fault zone, or (ii) they are brought to shallower levels during footwall uplift. Furthermore, we do not exclude the possible role of gabbro intrusion in the development of favorable local conditions for serpentinization. This early stage serpentinization, therefore, would produce a stable magnetization in a localized region immediately adjacent to the main detachment. Hence, samples recovered from close to the detachment surface [e.g., *MacLeod et al.*, 2011] will record substantial (or even the full history of) footwall rotation.

Serpentinization can start and continue only if space for volumetric expansion is available, otherwise reactions stop and their products seal and clog the fractures, restricting further water infiltration. Accordingly, serpentinization reactions that initially started along the detachment fault eventually propagate away from the fault plane, simultaneously with volumetric expansion related to progressive unloading during footwall unroofing and rotation [*Andreani et al.*, 2007]. During this phase, widespread faulting in the footwall in response to uplift and rotation may favor further water influx and serpentinization. The depth below the

detachment fault plane reached by serpentinization is therefore a function of both the geostatic pressure and local tectonic activity at the footwall. The deepening of serpentinization during footwall uplift and rotation should therefore be reflected in an age of magnetization that decreases away from the fault surface into the footwall. Serpentinization of deeper portions of a detachment footwall may be delayed until its complete unroofing and rotation, as seems to have been the case of the Mirdita OCC [*Maffione et al*., 2013; this study] and several samples from the Fifteen-Twenty Fracture Zone [*Garcés and Gee*, 2007]. Serpentinization reactions may then continue along secondary faults cutting the footwall after unroofing and rotation are complete, as suggested by the occurrence of serpentinization-driven, low-temperature hydrothermal systems, like the Lost City vent field at the MAR located some tens of kilometers off axis [e.g., *Kelley et al*., 2001; *Früh-Green et al*., 2003].

This model, however, should be applied carefully to individual cases where progressive migration of the serpentinization front into the footwall aided by small-scale cracking and faulting is likely to be coupled with rapid and localized serpentinization along major faults.

6. Conclusions

In this study, we integrated results from new rock magnetic, paleomagnetic, and petrological analyses of 144 variably serpentinized peridotite samples from a fossil oceanic core complex (OCC) preserved in the Mirdita ophiolite (Albania), with previously published data from 239 mid-ocean ridge-related abyssal peridotite samples collected at various scientific ocean drilling sites (DSDP and ODP). This yielded an updated, comprehensive database of magnetic properties of mid-ocean ridge peridotites across the complete range of serpentinization degrees (0–100%). Variations in a range of magnetic parameters (magnetite content, natural remanent magnetization (NRM), magnetic susceptibility, coercivity, hysteresis parameters) with the degree of serpentinization, and paleomagnetic data provide new constraints on the fundamental mechanisms and main products of serpentinization at divergent margins and its effect on the magnetization of the oceanic lithosphere.

An exponential increase of NRM, magnetic susceptibility, and magnetite content during serpentinization implies a major change in alteration conditions from rock-dominated to fluid-dominated systems at a critical serpentinization threshold of ~60%. We suggest that this transition is caused by a dramatic increase in transient permeability due to a pervasive mechanical weakening of the reacting rock during serpentinization.

The grain size of magnetite formed during serpentinization is also directly correlated with the progression of the serpentinization reaction. Very fine, super-paramagnetic (SP) particles are formed during the initial stages of serpentinization (<10%), whereas mainly single-domain (SD) magnetite is produced up to ~40% reaction progression, and possibly from the very beginning of the alteration process. Substantial production of pseudo-single-domain (PSD), and multidomain (MD) grains occurs at ~40% and ~60% reaction progress onward, respectively.

The grain-size of newly formed magnetite during serpentinization has direct implications for the nature of remanence carrying phases that are relevant to understanding potential contributions of mid-ocean ridge-related serpentinized peridotites to marine magnetic anomalies. SD and PSD magnetite grains, mostly produced during the initial stages of serpentinization (<~60% reaction completion) within pervasive sets of thin veins, can carry stable magnetizations. The MD fraction, mainly formed within sparse, larger veins at later serpentinization stages (>~60% reaction completion), carries only scattered low stability components. This evidence, together with variable Königsberger ratios, suggests that variably serpentinized peridotites are unlikely to contribute to regionally coherent patterns of oceanic magnetic anomalies.

Finally, a model for the evolution of serpentinization at OCCs is proposed, based on new paleomagnetic data from the fossil Mirdita OCC of Albania. Serpentinization of an embryonic OCC initiates at the detachment surface, affecting the footwall immediately adjacent (within a few tens of meters) to the fault plane. The serpentinization front progressively moves into the footwall and away from the detachment surface as a result of unloading and pressure release during footwall unroofing. Serpentinized peridotites close to the detachment surface acquire their remanence early in the evolution of the OCC and may record substantial footwall rotation, whereas rocks deeper in the footwall may undergo serpentinization after (near) complete unroofing and rotation.

Acknowledgments
This work was funded by an FP7 Marie Curie IEF fellowship to M. Maffione, A. Morris, and M. W. Anderson. M. Maffione and D.J.J. van Hinsbergen acknowledge funding through an ERC Starting grant (to DJJvH, project 306810—SINK) and an NWO VIDI grant. O.P. acknowledges an NWO VENI grant. The original manuscript has been significantly improved thanks to constructive comments of the Editor Thorsten Becker, Associate Editor Barbara John, besides Ronald Frost and two additional anonymous reviewers.

References

Allerton, S., and M. Tivey (2001), Magnetic polarity structure of the lower oceanic crust, *Geophys. Res. Lett.*, *28*, 423–426, doi:10.1029/2000GL008493.

Alt, J. C., and W. C. Shanks (1998), Sulfur in serpentinized oceanic peridotites: Serpentinization processes and microbial sulfate reduction. *J. Geophys. Res.*, *103*, 9917–9929.

Alt, J., et al. (2009), Drilling in Serpentine Sea, White Paper "Serpentine Sea" presented at the INVEST conference, Bremen, 23–25 Sep.

Andreani, M., C. Mével, A. M. Boullier, and J. Escartín (2007), Dynamic control on serpentine crystallization in veins: Constraints on hydration processes in oceanic peridotites, *Geochem. Geophys. Geosyst.*, *8*, Q02012, doi:10.1029/2006GC001373.

Bach, W., C. J. Garrido, H. Paulick, J. Harvey, and M. Rosner (2004), Seawater-peridotite interactions: First insights from ODP Leg 209, MAR 15°N, *Geochem. Geophys. Geosyst.*, *5*, Q09F26, doi:10.1029/2004GC000744.

Bach, W., H. Paulick, C. J. Garrido, B. Ildefonse, W. P. Meurer, and S. E. Humphris (2006), Unraveling the sequence of serpentinization reactions: Petrography, mineral chemistry, and petrophysics of serpentinites from MAR 15°N (ODP Leg 209, Site 1274), *Geophys. Res. Lett.*, *33*, L13306, doi:10.1029/2006GL025681.

Baines, A. G., M. J. Cheadle, B. B. John, and J. J. Schwartz (2008), The rate of oceanic detachment faulting at Atlantis Bank, SW Indian Ridge, *Earth Planet. Sci. Lett.*, *273*(1–2), 105–114, doi:10.1016/j.epsl.2008.06.013.

Beard, J. S., B. R. Frost, P. Fryer, A. McCaig, R. Searle, B. Ildefonse, P. Zinin, and S. K. Sharma (2009), Onset and progression of serpentinization and magnetite formation in olivine-rich troctolite from IODP Hole U1309D, *J. Petrol.*, *50*(3), 387–403, doi:10.1093/petrology/egp004.

Beltrando, M., G. Frasca, R. Compagnoni, and A. Vitale-Brovarone (2012), The Valaisan controversy revisited: Multi-stage folding of a Mesozoic hyper-extended margin in the Petit St. Bernard pass area (Western Alps), *Tectonophysics*, *579*, 17–36, doi:10.1016/j.tecto.2012.02.010.

Besse, J., and V. Courtillot (2002), Apparent and true polar wander and the geometry of the geomagnetic field over the last 200 Myr, *J. Geophys. Res.*, *107*(B11), 2300.

Bina, M. M., and B. Henry (1990), Magnetic properties, opaque mineralogy and magnetic anisotropies of serpentinized peridotites from ODP Hole 670A near the Mid-Atlantic Ridge, *Phys. Earth Planet. Inter.*, *65*(1–2), 88–103.

Blackman, D., B. Ildefonse, B. John, Y. Ohara, D. Miller, and C. MacLeod (2006), Oceanic core complex formation, Atlantis Massif, *Proc. Ocean Drill. Program Sci. Results*, 304/305, http://dx.doi.org/10.2204/iodp.proc.304305.2006.

Bortolotti, V., and G. Principi (2005), Tethyan ophiolites and Pangea breakup, *Isl. Arc*, *14*, 442–470.

Bortolotti, V., A. Kodra, M. Marroni, F. Mustafa, L. Pandolfi, G. Principi, and E. Saccani (1996), Geology and petrology of ophiolitic sequences in the Mirdita region (northern Albania), *Ofioliti*, *21*(1), 3–20.

Bortolotti, V., M. Chiari, M. Marroni, L. Pandolfi, G. Principi, and E. Saccani (2013), Geodynamic evolution of ophiolites from Albania and Greece (Dinaric-Hellenic belt): One, two, or more oceanic basins?, *Int. J. Earth Sci.*, *102*(3), 783–811, doi:10.1007/s00531-012-0835-7.

Boschi, C., G. L. Früh-Green, A. Delacour, J. A. Karson, and D. S. Kelley (2006), Mass transfer and fluid flow during detachment faulting and development of an oceanic core complex, Atlantis Massif (MAR 30°N), *Geochem. Geophys. Geosyst.*, *7*, Q01004, doi:10.1029/2005GC001074.

Buck, W. R. (1988), Flexural rotation of normal faults, *Tectonics*, *7*, 959–973.

Cann, J. R., D. K. Blackman, D. K. Smith, E. McAllister, B. Janssen, S. Mello, E. Avgerinos, A. R. Pascoe, and J. Escartín (1997), Corrugated slip surfaces formed at ridge-transform intersections on the Mid-Atlantic Ridge, *Nature*, *385*(6614), 329–332.

Cannat, M., et al. (1995), Thin crust, ultramafic exposures, and rugged faulting patterns at the Mid-Atlantic Ridge (22°–24°N), *Geology*, *23*(1), 49–52, doi:10.1130/0091–7613(1995)023<0049:TCUEAR>2.3.CO;2.

Cannat, M., D. Sauter, V. Mendel, E. Ruellan, K. Okino, J. Escartin, V. Combier, and M. Baala (2006), Modes of seafloor generation at a melt-poor ultraslow-spreading ridge, *Geology*, *34*(7), 605–608, doi:10.1130/G22486.1.

Cannat, M., D. Sauter, A. Bezos, C. Meyzen, E. Humler, and M. Le Rigoleur (2008), Spreading rate, spreading obliquity, and melt supply at the ultraslow spreading Southwest Indian Ridge, *Geochem. Geophys. Geosyst.*, *9*, Q04002, doi:10.1029/2007GC001676.

Chadima, M., and F. Hrouda (2006), Remasoft 3.0 a user-friendly paleomagnetic data browser and analyzer, *Trav. Géophys.*, *XXVII*, 20–21.

Christensen, N. I. (1978), Ophiolites, seismic velocities and oceanic crustal structure, *Tectonophysics*, *47*, 131–157.

Coleman, R. G., and T. E. Keith (1971), A chemical study of serpentinization-burro mountain, California, *J. Petrol.*, *12*(2), 311–328.

Day, R., M. Fuller, and V. A. Schmidt (1977), Hysteresis properties of titanomagnetites: Grain-size and compositional dependence, *Phys. Earth Planet. Inter.*, *13*(4), 260–267.

Dilek, Y. (2010), Eastern Mediterranean geodynamics, *Int. Geol. Rev.*, *52*(2–3), 111–116, doi:10.1080/00206810902951031.

Dilek, Y., M. Shallo, and H. Furnes (2005), Rift-Drift, seafloor spreading, and subduction tectonics of Albanian ophiolites, *Int. Geol. Rev.*, *47*(2), 147–176, doi:10.2747/0020–6814.47.2.147.

Dilek, Y., H. Furnes, and M. Shallo (2008), Geochemistry of the Jurassic Mirdita Ophiolite (Albania) and the MORB to SSZ evolution of a marginal basin oceanic crust, *Lithos*, *100*(1–4), 174–209, doi:10.1016/j.lithos.2007.06.026.

Dimo-Lahitte, A., P. Monié, and P. Vergély (2001), Metamorphic soles from the Albanian ophiolites: Petrology, 40Ar/39Ar geochronology, and geodynamic evolution, *Tectonics*, *20*, 78–96, doi:10.1029/2000TC900024.

Dunlop, D. J. (2002), Theory and application of the Day plot (Mrs/Ms versus Hcr/Hc). 1: Theoretical curves and tests using titanomagnetite data, *J. Geophys. Res.*, *107*(3), 4–1–4–22, doi:10.1029/2001JB000486.

Dunlop, D. J., and Ö. Özdemir (1997), *Rock Magnetism: Fundamentals and Frontiers, Cambridge Stud. Magn.*, 573 pp., Cambridge Univ. Press, Cambridge, U. K.

Dyment, J., J. Arkani-Hamed, and A. Ghods (1997), Contribution of serpentinized ultramafics to marine magnetic anomalies at slow and intermediate spreading centers: Insights from the shape of the anomalies, *Geophys. J. Int.*, *129*, 691–701.

Escartín, J., and J. P. Canales (2011), Detachments in oceanic lithosphere: Deformation, magmatism, fluid flow, and ecosystems, *Eos Trans. AGU*, *92*(4), 31.

Escartín, J., G. Hirth, and B. Evans (1997), Effects of serpentinization on the lithospheric strength and the style of normal faulting at slow-spreading ridges, *Earth Planet. Sci. Lett.*, *151*(3–4), 181–189.

Escartín, J., G. Hirth, and B. Evans (2001), Strength of slightly serpentinized peridotites: Implications for the tectonics of oceanic lithosphere, *Geology*, *29*(11), 1023–1026, doi:10.1130/0091–7613(2001)029<1023:SOSSPI>2.0.CO.

Escartín, J., D. K. Smith, J. Cann, H. Schouten, C. H. Langmuir, and S. Escrig (2008), Central role of detachment faults in accretion of slow-spreading oceanic lithosphere, *Nature*, *455*(7214), 790–794, doi:10.1038/nature07333.

Evans, B. W. (2004), The serpentinite multisystem revisited: Chrysotile is metastable, *Int. Geol. Rev.*, *46*(6), 479–506, doi:10.2747/0020–6814.46.6.479.

Evans, B. W. (2008), Control of the products of serpentinization by the $Fe^{2+}Mg^{-1}$ exchange potential of olivine and orthopyroxene, *J. Petrol.*, *49*(10), 1873–1887, doi:10.1093/petrology/egn050.
Frost, B. R., K. A. Evans, S. M. Swapp, J. S. Beard, and F. E. Mothersole (2013), The process of serpentinization in dunite from New Caledonia, *Lithos*, *178*, 24–39, doi:10.1016/j.lithos.2013.02.002.
Frost, R. B., and J. S. Beard (2007), On silica activity and serpentinization, *J. Petrol.*, *48*(7), 1351–1368, doi:10.1093/petrology/egn026.
Früh-Green, G. L., D. S. Kelley, S. M. Bernasconi, J. A. Karson, K. A. Ludwig, D. A. Butterfield, C. Boschi, G. Proskurowski (2003), 30,000 Years of hydrothermal activity at the Lost City Vent Field, *Science*, *301*(5632), 495–498, doi:10.1126/science.1085582.
Garcés, M., and J. S. Gee (2007), Paleomagnetic evidence of large footwall rotations associated with low-angle faults at the Mid-Atlantic Ridge, *Geology*, *35*(3), 279, doi:10.1130/G23165A.1.
Gee, J. S., and D. V. Kent (2007), 5.12—Source of oceanic magnetic anomalies and the geomagnetic polarity timescale, in *Treatise on Geophysics*, edited by G. Schubert, pp. 455–507, Elsevier, Amsterdam.
Grimes, C. B., B. E. John, M. J. Cheadle, and J. L. Wooden (2008), Protracted construction of gabbroic crust at a slow spreading ridge: Constraints from 206Pb/238U zircon ages from Atlantis Massif and IODP Hole U1309D (30_N, MAR), *Geochem. Geophys. Geosyst.*, *9*, Q08012, doi:10.1029/2008GC002063.
Harrison, R. J., and J. M. Feinberg (2008), FORCinel: An improved algorithm for calculating first-order reversal curve distributions using locally weighted regression smoothing, *Geochem. Geophys. Geosyst.*, *9*, Q05016, doi:10.1029/2008GC001987.
Ildefonse, B., D. K. Blackman, B. E. John, Y. Ohara, D. J. Miller, and C. J. MacLeod (2007), Oceanic core complexes and crustal accretion at slow-spreading ridges, *Geology*, *35*(7), 623–626, doi:10.1130/G23531A.1.
Iyer, K., B. Jamtveit, J. Mathiesen, A. Malthe-Sørenssen, and J. Feder (2008), Reaction-assisted hierarchical fracturing during serpentinization, *Earth Planet. Sci. Lett.*, *267*(3–4), 503–516, doi:10.1016/j.epsl.2007.11.060.
Katayama, I., I. Kurosaki, and K.-I. Hirauchi (2010), Low silica activity for hydrogen generation during serpentinization: An example of natural serpentinites in the Mineoka ophiolite complex, central Japan, *Earth Planet. Sci. Lett.*, *298*, 199–204, doi:10.1016/j.epsl.2010.07.045.
Kelemen, P. B., and G. Hirth (2012), Reaction-driven cracking during retrograde metamorphism: Olivine hydration and carbonation, *Earth Planet. Sci. Lett.*, *345–348*, 81–89, doi:10.1016/j.epsl.2012.06.018.
Kelemen, P. B., E. Kikawa, D. J. Miller, and Shipboard Scientist (2004), *Proceedings of Ocean Drilling Program, Initial Reports*, *209*, Ocean Drill. Program, College Station, Tex., doi:10.2973/odp.proc.ir.209.101.2004.
Kelley, D. S., J. A., Karson, D. K. Blackman, G. L. Früh-Green, D. Butterfield, M. Lilley, M. Schrenk, E. Olson, K. Roe, and J. Lebon (2001), An off-axis hydrothermal vent field near the mid-Atlantic ridge at 30°N, *Nature*, *412*, 145–149, doi:10.1038/35084000.
Kelso, P. R., C. Richter, and J. E. Pariso (1996), Rock magnetic properties, magnetic mineralogy and paleomagnetism of peridotite from site 895, Hess Deep, *Proc. Ocean Drill. Program Sci. Results*, *147*, 405–413.
Klein, F., W. Bach, N. Jons, T. McCollom, B. Moskowitz, and T. Berquo (2009), Iron partitioning and hydrogen generation during serpentinization of abyssal peridotites from 15°N on the Mid-Atlantic Ridge, *Geochim. Cosmochim. Acta*, *73*(22), 6868–6893, doi:10.1016/j.gca.2009.08.021.
Klein, F., W. Bach, S. E. Humphris, W. A. Kahl, N. Jöns, B. Moskowitz, and T. S. Berquó (2014), Magnetite in seafloor serpentinite—Some like it hot, *Geology*, *42*, 135–138, doi:10.1130/G35068.1.
Lavier, L. L., W. R. Buck, and A. N. B. Poliakov (1999), Self-consistent rolling-hinge model for the evolution of large-offset low-angle normal faults, *Geology*, *27*(12), 1127–1130.
Liati, A., D. Gebauer, and C. M. Fanning (2004), The age of ophiolitic rocks of the Hellenides (Vourinos, Pindos, Crete): First U-Pb ion microprobe (SHRIMP) zircon ages, *Chem. Geol.*, *207*(3–4), 171–188, doi:10.1016/j.chemgeo.2004.02. 010.
Linert, B. R., and P. J. Wasilewski (1979), A magnetic study of the serpentinization process at Burro Mountain, California, *Earth Planet. Sci. Lett.*, *43*, 406–416.
MacLeod, C. J., et al. (2002), Direct geological evidence for oceanic detachment faulting: The Mid-Atlantic Ridge, 15°45′N, *Geology*, *30*(10), 879, doi:10.1130/0091–7613(2002)030<0879:DGEFOD>2.0.CO;2.
MacLeod, C. J., J. Carlut, J. Escartín, H. Horen, and A. Morris (2011), Quantitative constraint on footwall rotations at the 15°45′N oceanic core complex, Mid-Atlantic Ridge: Implications for oceanic detachment fault processes, *Geochem. Geophys. Geosyst.*, *12*, Q0AG03, doi:10.1029/2011GC003503.
Maffione, M., A. Morris, and M. W. Anderson (2013), Recognizing detachment-mode seafloor spreading in the deep geological past, *Sci. Rep.*, *3*, 2336, doi:10.1038/srep02336.
Malvoisin, B., J. Carlut, and F. Brunet (2012), Serpentinization of oceanic peridotites. 1: A high-sensitivity method to monitor magnetite production in hydrothermal experiments, *J. Geophys. Res.*, *117*, B01104, doi:10.1029/2011JB008612.
Mayergoyz, I. D. (1986), Mathematical models of hysteresis, *Phys. Rev. Lett.*, *56*(15), 1518–1521.
Ménez, B., V. Pasini, and D. Brunelli (2012), Life in the hydrated suboceanic mantle, *Nat. Geosci.*, *5*(2), 133–137, doi:10.1038/ngeo1359.
Meshi, A., F. Boudier, A. Nicolas, and I. Milushi (2010), Structure and tectonics of lower crustal and upper mantle rocks in the Jurassic Mirdita ophiolites, Albania, *Int. Geol. Rev.*, *52*(2–3), 117–141, doi:10.1080/00206810902823982.
Mével, C. (2003), Serpentinization of abyssal peridotites at mid-ocean ridges, *C. R. Geosci.*, *335*(10–11), 825–852, doi:10.1016/j.crte.2003.08.006.
Miller, D. J., and N. I. Christensen (1997), Seismic velocities of lower crustal and upper mantle rocks from the slow-spreading Mid-Atlantic Ridge, south of the Kane transform zone (MARK), *Proc. Ocean Drill. Program Sci. Results*, *153*, 437–454.
Mohn, G., G. Manatschal, M. Beltrando, E. Masini, and N. Kusznir (2012), Necking of continental crust in magma-poor rifted margins: Evidence from the fossil Alpine Tethys margins, *Tectonics*, *31*, TC1012, doi:10.1029/2011TC002961.
Moody, J. B. (1976), An experimental study on the serpentinization of iron-bearing olivines, *Can. Mineral.*, *14*, 462–478.
Morris, A., J. S. Gee, N. Pressling, B. E. John, C. J. MacLeod, C. B. Grimes, and R. C. Searle (2009), Footwall rotation in an oceanic core complex quantified using reoriented Integrated Ocean Drilling Program core samples, *Earth Planet. Sci. Lett.*, *287*(1–2), 217–228, doi:10.1016/j.epsl.2009.08.007.
Muxworthy, A. R., and E. McClelland (2000), Review of the low-temperature magnetic properties of magnetite from a rock magnetic perspective, *Geophys. J. Int.*, *140*(1), 101–114, doi:10.1046/j.1365-246X.2000.00999.x.
Nazarova, K. A. (1994), Serpentinized peridotites as a possible source for oceanic magnetic anomalies, *Mar. Geophys. Res.*, *16*(6), 455–462.
Nicolas, A., F. Boudier, and A. Meshi (1999), Slow spreading accretion and mantle denudation in the Mirdita ophiolite (Albania), *J. Geophys. Res.*, *104*, 15,155–15,167.
O'Hanley, D. S. (1996), *Serpentinites: Records of Tectonic and Petrologic History*, 277 pp., Oxford Univ. Press, Oxford, U. K.
Özdemir, Ö. (1990), High-temperature hysteresis and thermoremanence of single-domain maghemite, *Phys. Earth Planet. Int.*, *65*(1–2), 125–136.

Özdemir, Ö., D. J. Dunlop, and B. M. Moskowitz (1993), The effect of oxidation on the Verwey transition in magnetite, *Geophys. Res. Lett.*, *20*, 1671–1674.

Oufi, O., M. Cannat, and H. Horen (2002), Magnetic properties of variably serpentinized abyssal peridotites, *J. Geophys. Res.*, *107*(5), EPM 3–1–EPM 3–20, doi:10.1029/2001JB000549.

Paulick, H., W. Bach, M. Godard, J. C. M. De Hoog, G. Suhr, and J. Harvey (2006), Geochemistry of abyssal peridotites (Mid-Atlantic Ridge, 15°20′N, ODP Leg 209): Implications for fluid/rock interaction in slow spreading environments, *Chem. Geol.*, *234*, 179–210, doi:10.1016/j.chemgeo.2006.04.011.

Pike, C. R., A. P. Roberts, and K. L. Verosub (1999), Characterizing interactions in fine magnetic particle systems using first order reversal curves, *J. Appl. Phys.*, *85*(9), 6660–6667.

Plümper, O., H. E. King, C. Vollmer, Q. Ramasse, H. Jung, and H. Austrheim (2012a), The legacy of crystal-plastic deformation in olivine: High-diffusivity pathways during serpentinization, *Contrib. Mineral. Petrol.*, *163*(4), 701–724, doi:10.1007/s00410-011-0695-3.

Plümper, O., A. Røyne, A. Magraso, and B. Jamtveit (2012b), The interface-scale mechanism of reaction-induced fracturing during serpentinization, *Geology*, *40*, 1103–1106.

Prévot, M., A. Lecaille, and E. A. Mankinen (1981), Magnetic effects of maghemitization of oceanic crust, *J. Geophys. Res.*, *86*, 4009–4020.

Roberts, A. P., C. R. Pike, and K. L. Verosub (2000), First-order reversal curve diagrams: A new tool for characterizing the magnetic properties of natural samples, *J. Geophys. Res.*, *105*, 28,461–28,475.

Robertson, A., and M. Shallo (2000), Mesozoic-Tertiary tectonic evolution of Albania in its regional Eastern Mediterranean context, *Tectonophysics*, *316*(3–4), 197–254.

Robertson, A. H. F. (2012), Late Palaeozoic-Cenozoic tectonic development of Greece and Albania in the context of alternative reconstructions of Tethys in the Eastern Mediterranean region, *Int. Geol. Rev.*, *54*(4), 373–454, doi:10.1080/00206814.2010.543791.

Sauter, D., et al. (2013), Continuous exhumation of mantle-derived rocks at the Southwest Indian Ridge for 11 million years, *Nat. Geosci.*, *6*(4), 314–320, doi:10.1038/ngeo1771.

Schlinger, C. M. (1985), Magnetization of lower crust and interpretation of regional magnetic anomalies: Example from Lofoten and Vesteralen, Norway, *J. Geophys. Res.*, *90*, 11,484–11,502.

Schmid, S. M., D. Bernoulli, B. Fügenschuh, L. Matenco, S. Schefer, R. Schuster, M. Tischler, and K. Ustaszewski (2008), The Alpine-Carpathian-Dinaridic orogenic system: Correlation and evolution of tectonic units, *Swiss J. Geosci.*, *101*(1), 139–183.

Smith, D. K., J. Escartín, H. Schouten, and J. R. Cann (2008), Fault rotation and core complex formation: Significant processes in seafloor formation at slow-spreading mid-ocean ridges (Mid-Atlantic Ridge, 13°–15°N), *Geochem. Geophys. Geosyst.*, *9*, Q03003, doi:10.1029/2007GC001699.

Snow, J. E., and H. J. B. Dick (1995), Pervasive magnesium loss by marine weathering of peridotite, *Geochim. Cosmochim. Acta*, *59*, 4219–4235.

Tauxe, L. (2010), *Essentials of Paleomagnetism*, 489 pp., Univ. of Calif. Press, Berkeley.

Thompson, G., and W. G. Melson (1970), Boron contents of serpentinites and metabasalts in the oceanic crust: Implications for the boron cycle in the oceans, *Earth Planet. Sci. Lett.*, *8*, 61–65.

Toft, P. B., J. Arkani-Hamed, and S. E. Haggerty (1990), The effects of serpentinization on density and magnetic susceptibility: A petrophysical model, *Phys. Earth Planet. Inter.*, *65*(1–2), 137–157.

Toljic, M., L. Matenco, M. N. Ducea, U. Stojadinovič, J. Milivojevič, and N. Derič (2013), The evolution of a key segment in the Europe-Adria collision: The fruška gora of northern serbia, *Global Planet. Change*, *103*(1), 39–62, doi:10.1016/j.gloplacha.2012.10.009.

Tremblay, A., A. Meshi, and J. H. Bédard (2009), Oceanic core complexes and ancient oceanic lithosphere: Insights from Iapetan and Tethyan ophiolites (Canada and Albania), *Tectonophysics*, *473*(1–2), 36–52, doi:10.1016/j.tecto.2008.08.003.

Tucholke, B. E., J. Lin, and M. C. Kleinrock (1998), Megamullions and mullion structure defining oceanic metamorphic core complexes on the Mid-Atlantic Ridge, *J. Geophys. Res.*, *103*, 9857–9866.

van Hinsbergen, D. J. J., E. Hafkenscheid, W. Spakman, J. E. Meulenkamp, and R. Wortel (2005), Nappe stacking resulting from subduction of oceanic and continental lithosphere below Greece, *Geology*, *33*(4), 325–328, doi:10.1130/G20878.1.

Vissers, R. L. M., D. J. J. van Hinsbergen, P. Th. Meijer, and G. Piccardo (2013), Kinematics of Jurassic ultra-slow spreading in the Piemonte-Ligurian ocean, *Earth Planet. Sci. Lett.*, *380*, 138–150.

Zijderveld, J. D. A. (1967), A. C. demagnetization of rocks: Analysis of results, in *Methods in Palaeomagnetism*, edited by D. W. Collinson, K. M. Creer, and S. K. Runcorn, pp. 254–286, Elsevier, New York.